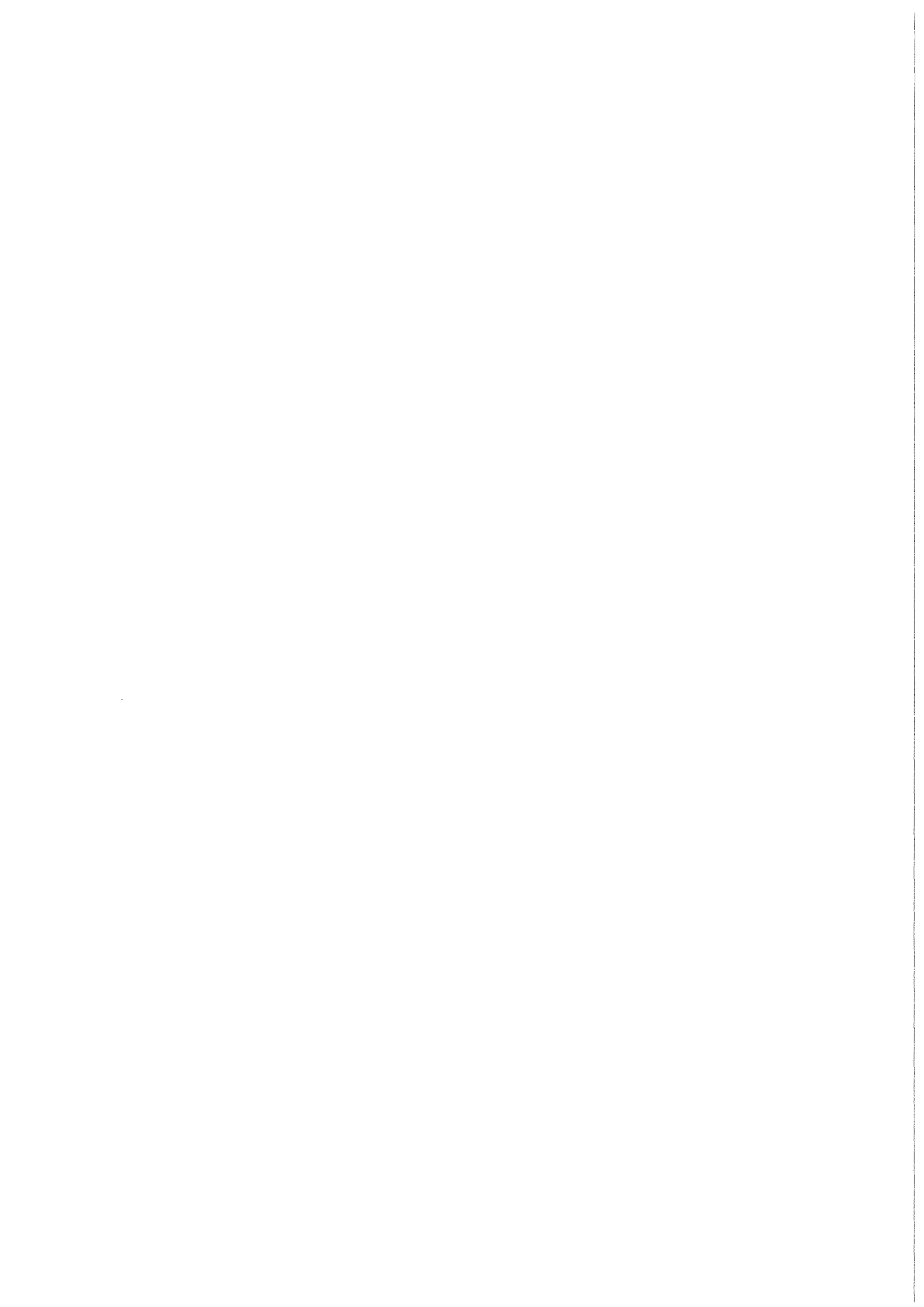


KfK 3839
Dezember 1984

Study of MHD Problems in Liquid Metal Blankets of Fusion Reactors

I. Michael
Institut für Reaktorbauelemente
Projekt Kernfusion

Kernforschungszentrum Karlsruhe



Kernforschungszentrum Karlsruhe
Institut für Reaktorbauelemente
Projekt Kernfusion

KfK 3839

Study of MHD Problems in Liquid Metal
Blankets of Fusion Reactors

I. Michael



Kernforschungszentrum Karlsruhe GmbH, Karlsruhe

Als Manuskript vervielfältigt
Für diesen Bericht behalten wir uns alle Rechte vor

Kernforschungszentrum Karlsruhe GmbH
ISSN 0303-4003

Abstract

This study describes in a concise form the state of knowledge regarding MHD problems to be expected in case of use of liquid metal in the blankets of fusion reactors with magnetic confinement. MHD pressure losses and MHD friction coefficients in the straight channel, in bent sections and in case of variation of the channel cross section play a major role because the high MHD flow resistances call for high pumping powers. Influencing the velocity profile transverse to the main flow direction of the liquid metal by application of an external, strong magnetic field bears consequences on the release and transport of corrosion products in the liquid metal circuit and on the heat transfer. Possibilities of reducing the MHD effects are discussed.

However, it becomes obvious that an account of the lack of experimental results there are still major gaps in the knowledge of MHD effects occurring in strong magnetic fields. These gaps can be greatly reduced by implementation of an experimental program as proposed in this report.

Zusammenfassung

Studie über MHD-Probleme im Flüssigmetall-Blanket von Fusionsreaktoren

Die Studie beschreibt in geraffter Form den Kenntnisstand der MHD-Probleme, wie sie bei der Verwendung von Flüssigmetall im Blanket von Fusionsreaktoren mit magnetischem Einschluß zu erwarten sind. Dabei spielen die MHD-Druckverluste und die -Reibungsbeiwerte im geraden Kanal, im Krümmer und bei Änderung des Kanalquerschnittes eine wesentliche Rolle, weil die hohen MHD-Strömungswiderstände hohe Pumpleistungen erfordern. Die Beeinflussung des Geschwindigkeitsprofils quer zur Hauptströmungsrichtung des Flüssigmetalls durch ein äußeres starkes Magnetfeld hat Konsequenzen auf Freisetzung und Transport von Korrosionsprodukten im Flüssigmetallkreislauf und auf den Wärmeübergang. Möglichkeiten zur Minderung der MHD-Effekte werden erörtert.

Es zeigt sich jedoch, daß durch das Fehlen ausreichender experimenteller Ergebnisse der MHD-Effekte in starken Magnetfeldern noch deutliche Lücken im Kenntnisstand bestehen. Diese Lücken könnten durch ein experimentelles Programm, das vorgeschlagen wird, wesentlich reduziert werden.

1. The Problem

Since about 20 years concepts and studies have been presented with liquid metal contained in the blankets of fusion reactors. The liquid metal is used as the coolant and as the tritium breeding material but also as the breeding material alone. But other concepts have been proposed as well which do without any liquid metal in the blanket. An essential criterion of deciding in favor of or against the use of liquid metal are the interactions establishing with the strong magnetic plasma holding fields of fusion reactors. The considerations and estimates concerning these magneto-hydrodynamic (MHD)-effects are still well underway. This report will provide a concise survey of the problems connected with MHD effects.

The previous studies of MHD problems in liquid metal flows have concentrated on the determination of the pressure drop in the flow in straight pipes perpendicular to the magnetic field. Pressure losses in pipe bends and in magnetic fields subject to local variations have been investigated in a few cases only.

On the whole, only very few activities have been devoted to the attempt of determining the velocity distribution in a liquid metal flow exposed to a magnetic field. However, this velocity distribution in a liquid metal blanket exerts a decisive influence on heat and mass transport. Therefore, knowledge of this distribution is required also for working out concepts in which the liquid metal does not serve as the coolant but solely as the breeding material. Also in this context the questions of material corrosion and tritium transport are of high importance.

Experience published so far in this field of research activities is limited by the MHD effects being partly correlated nonlinearly and the experimental studies performed so far as well as the results derived from them being obtained in small B-fields compared with the magnetic plasma holding fields. The main reason probably is that experimenting in high magnetic fields is relatively expensive both in terms of plant design and operating costs. Therefore, only few experimental facilities are available worldwide in which high magnetic fields can be generated.

The lack of experimental results on liquid metal flow in high magnetic fields restricts the transferability of theoretical findings which have been validated only for low magnetic fields.

2. Principles of MHD Flow

Four major effects can be distinguished which act upon a magnetic field perpendicular to the flow of an electrically conducting fluid; mostly they occur coupled with each other:

- Electric eddy currents flow in a plane perpendicular to the main direction of flow. They cause the thickness of the wall boundary layer to decrease and wall friction to increase (Hartmann effect).

- If the channel wall is electrically conducting, the eddy currents are back-circuited via this wall. This gives rise to electromagnetic volume forces counteracting the fluid motion.

- When the channel flow enters and leaves the homogeneous magnetic field zone, i.e., in the field boundary zones, eddy currents are generated which likewise cause pressure losses counteracting the flow.
- Another effect occurring both in the fluid flowing transversally and in the fluid flowing parallel to the magnetic field cause turbulence suppression, this lamination leading to an increase in the critical Reynolds number.

The basic equations describing MHD flow are:

- The Ohm law applicable to the current of charged particles in general in an electric and in a magnetic field reads:

$$\vec{j} = \sigma(\vec{E} + \vec{U} \times \vec{B}) \quad (1)$$

The Maxwell equations of electrodynamics must be added, namely

$$\nabla \times \vec{E} = 0 \quad (2)$$

$$\nabla \cdot \vec{B} = 0 \quad (3)$$

$$\nabla \times \vec{B} = \mu_0 \cdot \vec{j} \quad (4)$$

\vec{j} = electric current density

- the momentum equation

$$\nabla p = \eta \cdot \nabla^2 \vec{u} + \vec{j} \times \vec{B} \quad (5)$$

- and the continuity equation

$$\dot{m} = \rho \cdot \bar{u} \cdot A = \text{const.} \quad (6)$$

The dimensionless characteristics important for the channel flow of an electrically conducting fluid are:

the Reynolds number $Re = \frac{\bar{u} \cdot d_H \cdot \rho}{\eta}$

and in the magnetic field B:

the Hartmann number $M = a \cdot B \sqrt{\frac{\sigma}{\eta}}$

the electrical conductance coefficient $\phi = \frac{\sigma_w \cdot t_w}{\sigma \cdot a}$

and the magnetic Reynolds number $R_m = \sigma \cdot \bar{u} \cdot d \cdot \mu$

where \bar{u} is the mean fluid velocity, $d_H = 2a$ is the hydraulic diameter, η is the dynamic viscosity, and μ is the magnetic permeability. Depending on the orientation, B is the field strength of magnetic induction $\vec{B} \perp \vec{u}$ or $\vec{B} \parallel \vec{u}$. The conductance coefficient is determined by the electrical conductivity σ_w of the channel wall and by σ of the liquid metal, t_w being the wall thickness. The critical Reynolds number Re_c for the transition from laminar to turbulent flow is 2300 in smooth pipes. The Hartmann number M is the dimensionless ratio of magnetic to hydrodynamic viscosity.

Last but not least, the magnetic Reynolds number constitutes the ratio of the induced magnetic field entrained with the fluid to the external magnetic field. R_m will be $\ll 1$ in channel flow in the fusion blanket and Eq. (4) can be neglected.

3. MHD Pressure Losses and MHD Friction Coefficients

3.1 MHD Pressure Losses in Channel Flow

Starting from Hartmann's theory of MHD channel flow, Hoffman and Carlson [1, 2] proposed the following solution for the dimensionless pressure loss P_M :

$$P_M = \frac{a^2}{\eta \cdot \bar{u}} \left(- \frac{dp}{dx} \right) = \frac{M^2 \cdot \tanh M}{M - \tanh M} + \frac{M^2 \cdot \phi}{1 + \phi}; \quad (7)$$

This gives for great Hartmann numbers $M \gg 1$,

$$\frac{dp}{dx} = \frac{\eta \cdot \bar{u}}{a^2} (M + M^2 \frac{\phi}{1 + \phi}) \quad (8)$$

If the wall is metallicity conducting, i.e., $\phi \ll 1$,

$$\frac{\phi}{1 + \phi} \approx \phi \text{ and}$$

$$\frac{dp}{dx} = - \frac{\eta \cdot \bar{u}}{a^2} \cdot M^2 \phi = - \bar{u} \cdot B^2 \cdot \sigma \cdot \phi \quad (9)$$

If the channel wall is insulated electrically, we obtain for $\phi \rightarrow 0$

$$\frac{dp}{dx} = - \frac{\eta \cdot \bar{u}}{a^2} \cdot M \quad (10)$$

i.e., the pressure gradient still depends but linearly on the Hartmann number.

3.2 Example of Estimating the Pressure Losses in the Pipe Section of a Lithium Supply Manifold for $B = 0$ and $B = 10 \text{ T}$ [3]

1. Δp for $B = 0$ tesla

$$\Delta p = -\lambda \circ \frac{\ell}{d_H} \cdot \frac{\rho}{2} \cdot \bar{u}^2 \quad (11)$$

$$Re_{0.43} = \frac{\bar{u} \cdot d_H}{\gamma} = 5.26 \times 10^4$$

$$\begin{aligned} \Delta p &= 1.46 \times 10^{-1} \text{ Nm}^{-2} \\ &= 1.46 \times 10^{-4} \text{ bar} \\ &===== \end{aligned}$$

$$\rho_{\text{Li},400^{\circ}\text{C}} = 495 \text{ kg} \cdot \text{m}^{-3}$$

$$\gamma_{\text{Li},400^{\circ}\text{C}} = 81.7 \times 10^{-8} \text{ m}^2 \cdot \text{s}^{-1}$$

$$a = 0.05 \text{ m}, d_{\text{H}} = 0.1 \text{ m}$$

$$t = 0.0025 \text{ m}$$

$$l = 1 \text{ m}$$

$$\bar{u} = 0.43 \text{ m} \cdot \text{s}^{-1}$$

$$\lambda = 0.032$$

2. Δp_{B} for $B = 10$ tesla

$$\Delta p_{\text{B}} = \bar{u} \cdot \phi \cdot B_{\text{Y}}^2 \cdot \sigma_{\text{Li}} \cdot l \quad (12)$$

$$= 2.365 \text{ MN} \cdot \text{m}^{-2}$$

$$= 23.65 \text{ bar}$$

=====

$$\sigma_{\text{W},400^{\circ}\text{C}} = 1.1 \times 10^6 \text{ A}(\text{Vm})^{-1}$$

$$\sigma_{\text{Li},400^{\circ}\text{C}} = 2.2 \times 10^6 \text{ A}(\text{Vm})^{-1}$$

$$\phi = \frac{\sigma_{\text{W}} \cdot t}{\sigma_{\text{Li}} \cdot a} = 0.025$$

$$M = 35000$$

$$N = \frac{M^2}{\text{Re}} = 23300$$

$$\frac{\Delta p_{\text{R}}}{\Delta p} = \frac{23.65}{1.46 \times 10^{-4}} = 1.62 \times 10^5.$$

The CULHAM concept [3] of a lithium liquid metal cooled Tokamak system is based on a plasma holding field of ten tesla. A pressure loss in the supply manifold of 23.7 bar corresponds to this value. Later design concepts rely on clearly lower magnetic field strengths. Figure 1 shows how the MHD pressure loss decreases with the magnetic field, e.g., at 6 T to 8.5 bar.

3.3 MHD Friction Coefficient

From the relation describing the isothermal pressure drop in the absence of an external magnetic field

$$\frac{dp}{dx} = -\lambda_o \cdot \frac{1}{d_H} \cdot \frac{\rho}{2} \cdot \bar{u}^2 \quad (13)$$

the friction coefficient follows as

$$\lambda_o = - \frac{dp}{dx} \cdot \frac{2d_H}{\rho \cdot \bar{u}^2} \quad , \quad (14)$$

with $d_H = 4A/U$ being the hydraulic diameter. A is the channel cross section and U the wetted contour.

In case of laminar flow

$$\lambda_o = \frac{64}{Re} \quad (15)$$

and for turbulent flow the empirical formula proposed by Blasius applies to the range of $2300 < Re < 10^5$

$$\lambda_o = \frac{0,316}{Re^{-0,25}} \quad (16)$$

The flow of an incompressible electrically conducting fluid in a magnetic field is described by the setup

$$\lambda_M = f(M/Re). \quad (17)$$

For a great number of flow configurations Lielausis [4] listed the relations belonging to Eq. (17). They are entered in Table 3. (It should be noted that in these tables the

Hartmann number is designated Ha instead of M and the Stuart number - also termed interaction parameter - is $N = Ha^2/Re.$)

Although this compilation is quite helpful, the range of validity of the relations of the friction coefficients is given for some cases only. The original literature must be referred to in a number of instances. For channel flow perpendicular to the magnetic field and for high wall conductivity, $\phi \gg 1$ and $M \gg 1$, we obtain

$$\lambda_M = \frac{2M^2}{Re} \quad (18)$$

for the insulated wall, $\phi = 0$ and $M \gg 1$, we obtain

$$\lambda_M = \frac{2M}{Re} \quad (19)$$

For the flow in a pipe with conducting wall and $M \gg 1$ Branover [5] proposes the following relation of general validity

$$\frac{\lambda}{\lambda_0} = \frac{\pi \cdot M}{8(1+\phi)} \left\{ \frac{\pi}{\phi M} - \frac{4}{(\phi M)^2} + \frac{2}{(\phi M)^3} - \frac{4 \ln[\phi \cdot M + \sqrt{(\phi \cdot M)^2 - 1}]}{(\phi M)^3 \sqrt{(\phi \cdot M)^2 - 1}} \right\}^{-1} \quad (20)$$

Branover compares this theoretical relation with some experimental values for mercury flow in a copper pipe [6]. For these low friction coefficients the agreement of theory and experiment is relatively good ($\leq 2.5\%$); Fig. 6. The Reynolds number is $< 10^4$, the Hartmann number < 150 , and the conductance coefficient is between $1 < \phi < 20$.

Carre et al. [7] compare for a lithium cooled Tokamak reactor with the typical values

$$Re = 5 \times 10^4, M = 1 \times 10^5 \text{ and } \phi = 5 \times 10^{-2}$$

the friction coefficient ratios λ_M/λ_0 for laminar or turbulent channel flow and electrical wall conduction and wall insulation, respectively, entered in Table 3. The following findings are evident from Table 3:

- Between the ideal electrical wall conduction ($\phi = \infty$) in the channel and insulated wall ($\phi = 0$) the ratio $\lambda_M/\lambda_0 = 20,000$. The value of conduction at the steel wall of $\phi \sim 5 \times 10^{-2}$ lies between these extreme values.
- A low conductivity layer on the channel inner wall formed by corrosion deposits may lead both to a reduction in the values of λ_M and in the ratio dp/dx .

3.4 Restriction of the MHD Pressure Losses by Stresses in the Wall

The admissible MHD pressure losses are restricted by the mechanical stresses which they generate in the channel wall. For a thin-walled pipe $t \ll a$ the hoop stress f is obtained according to

$$f = \frac{a \cdot p}{t} \quad , \quad (21)$$

with a being the pipe radius, p the coolant pressure, and t the thickness of the pipe wall. If one starts from the MHD pressure gradients and the volume flow rate, one obtains

$$\begin{aligned} \frac{dp}{dx} &= - Q \cdot \sigma \cdot B^2 \cdot \phi \cdot \frac{1}{A} \\ &= - Q \cdot \sigma_w \cdot t \cdot B^2 \cdot \frac{1}{a \cdot A} \end{aligned} \quad (22)$$

where A is the channel cross section, σ is the electric fluidity, and σ_w is the conductivity of the wall.

The volume flow rate Q of the liquid metal, required for heat removal, is then obtained as

$$Q = \frac{P_w \cdot A_w}{c_p \cdot \rho \cdot \Delta T} \quad (23)$$

where A_w is the fractional area of the first wall supplied with coolant via the coolant channel (area A), P_w is the mean thermal wall load, ΔT is the temperature rise, c_p is the specific heat, and ρ is the density of the liquid metal.

If the pressure loss is related to the overall channel length l running perpendicular to the B-field, the following expression is obtained for the mechanical maximum stress at the pipe inner wall f_w of the supply manifold

$$f_w = \frac{\sigma_w \cdot l \cdot B^2 \cdot P_w \cdot A_w}{c_p \cdot \rho \cdot \Delta T \cdot A} \quad (24)$$

Hancox and Booth [8] made this study for the 1971 CULHAM design concerning the lithium cooled 5 GW_{th} Tokamak reactor and showed the correlation existing between the load on the first wall, the admissible wall stresses f_{adm} and the field of the magnetic flux density B (Fig. 2). Table 1 gives the values of the yield strength and creep rupture strength of some pipe materials.

3.5 Flow Undergoing Changes in Direction

The passage through bends, especially elbows, might be accompanied by whirl detachment and possibly the formation of cavities. If such flow obstructions are exposed to thermal loading hot spots may occur. The theoretical treatment and the experimental investigations in this field are still inadequate.

Investigations of our own into the friction coefficients in liquid sodium flow through meander shaped channels (Fig. 3) have revealed the surprisingly great influence of a strong external magnetic field B [9] which is evident from the table below.

Table

<u>B(T)</u>	<u>Friction Coefficient</u>
4.2	5500
2.1	1800
0	3.1

The channel cross section was $4 \times 15 \text{ mm}^2$, the sodium temperature 400°C , and the fluid velocity $u = 0.26 \text{ m/s}$, $Re = 5000$.

These strong influences exerted by the magnetic fields on liquid metal bend flow are yet understood insufficiently. Both the small dimensions of the test section and that of the working space in the high field magnet have so far ruled out investigations involving differential flow probes.

3.6 Flow under Conditions of Channel Cross Section Variation and in the Inhomogeneous Magnetic Field

Besides the MHD pressure losses in straight channels and in bent sections pressure losses occur also if the channel cross section undergoes variations and in case of local changes of the field of magnetic induction. Both flow patterns can be roughly described by the general relation

$$-\Delta p = K_{pI} \cdot \sigma \cdot \bar{u} \cdot B^2 \cdot \ell^* \cdot N^{-m} \quad (25)$$

where $N = M^2/Re$ is the Stuart number, and m is an exponent to be determined experimentally, K_{pI} is a pressure loss coefficient, and ℓ^* is a characteristic length. For the variables K_{pI} and ℓ^* a basis of computation of general validity can be indicated. It must be derived from experimental studies.

Hofman and Carlson [2] proposed an analytically derived solution for the local variation of the field around the inflow and outflow parts of a homogeneous magnetic field

zone, i.e., for the boundary field zone. The characteristic length in this case equals the channel width perpendicular to the B-field vector, $l^* = b$.

The field conditions for MHD flow in the homogeneous and in the inhomogeneous boundary field zones are evident from the MHD model represented in Fig. 4. The top part shows the development of B in the homogeneous zone I and upon transition to the field-free zone II. In the homogeneous B field ($x < 0$) also the induced electric field strength E_z is homogeneous. In the boundary field B_y , for $x > 0$, E_z decreases towards zero. This decrease of the E-field leads to an angle of contact of the current density j_w in the $x - z$ plane extending over the nominal flow zone up to the boundary layer zone.

3.7 Diminishment of the MHD Pressure Losses

Two concepts are considered for diminishing the MHD pressure losses. One concept is determined by an advantageous channel routing, the other relies on the reduction of the electrical conductivity of the channel.

3.7.1 ANL Concept

The ANL concepts illustrated in Fig. 5 [10] implies the coolant flow to be transformed from the poloidal flow direction, characterized by slow velocity, to a toroidal flow in narrower channels surmounting the original channels and characterized by a higher velocity. The flow in the poloidal direction is almost perpendicular to the direction of the magnetic flux density of the plasma holding field and is associated with MHD pressure losses. Toroidal flow leads solely to hydrodynamic pressure losses. The higher flow velocity guarantees a good heat transfer.

The abrupt change of flow directions (poloidal-toroidal-poloidal) in the magnetic field is characteristic of the ANL concept. Firstly, this elbow constitutes under the aspect of design the point of maximum loading of the first wall. Secondly, the sharp deflection in the elbow might cause detachment of flow accompanied by the formation of hot spots. To counteract this process, guide plates or baffles could be installed in the deflection zone.

3.7.2 Insulation between Liquid and Wall

As has been shown by the example the pressure loss in the liquid metal flow may adopt very high values. Consequently, both the required pumping power and the mechanical stresses in the channel wall might become inadmissibly high. Reduction in stress by increasing the wall thickness is not possible because in non-insulated walls the pressure loss in a first approximation increases linearly with the wall thickness. A way out of this problem could consist in providing an electric insulation between the liquid metal and the supporting wall. Two methods are eligible. The most obvious idea would be to coat the inner side of the channel wall with an insulating material. However, no suitable material and coating technique have been found till this day to achieve an adequate service life if the wall is in contact with the liquid metal. Therefore, the second method is more promising under which the wall is given a sandwich structure. The liquid metal is in contact with a thin (about 1 mm thick) wall supported via an electrical insulator by the load carrying channel wall. This technique is applied above all for the supply and return manifolds of the blanket because the radiation exposure of the insulator is negligibly small in these manifolds [10].

4. Influence of the Magnetic Fields on the Distribution of Flow Velocities

4.1 Fundamentals

A liquid metal flow perpendicular to an external magnetic field is leveled off in its flow profile. This applies on condition that the flow has developed into a hydrodynamic flow and the channel is not conducting electrically. Stephan solved the MHD momentum equation, which he made dimensionless by suitable standardization in a cylindrical geometry using modified Bessel and MacDonald functions [11]. The graphical representation of this solution is shown in Fig. 7 where $Y = r/R$ is the radial local coordinate, $U = u/\bar{u}$ is the dimensionless velocity, and M is the Hartmann number. With increasing Hartmann number the velocity profile is more and more leveled off perpendicular to the B-field intensity. This is paralleled by the development of a boundary layer of decreasing thickness which is termed also the Hartmann boundary layer.

Figure 8 shows for MHD flow the electric current paths in round and rectangular channels without and with electrical conduction of the walls. In addition, the relations between the thicknesses of the Hartmann boundary layers σ are indicated for non-conducting channel walls. For round pipes the boundary layer thickness near the wall components $\perp \vec{B}$ [3] reads

$$\delta \sim (a/M \cos\theta) \quad (26)$$

where θ is the angle between the normal to the wall \vec{n} and \vec{B} . For wall components $\parallel \vec{B}$ we obtain

$$\delta \sim (a/M^{2/3}) \quad (27)$$

For rectangular pipes the following relation holds for the wall normal to \vec{B}

$$\delta \sim (a/M^{-1}) \quad (28)$$

and for the parallel wall

$$\delta \sim (a/M^{-2}) \quad (29)$$

4.2 Destabilizing Effects in MHD Flow

The MHD volume forces K in the homogeneous magnetic field and in straight channels with a homogeneous conductivity of the wall, according to the relations

$$\vec{u} \times \vec{B} = \vec{E} \quad (30)$$

and

$$\vec{j} \times \vec{B} = \vec{K} \quad (31)$$

are exactly opposed to the flow of an electrically conducting fluid. If sudden disturbances occur in this system, this leads to destabilization in MHD flow. Disturbances might be:

- Sharp edged flow in bent sections accompanied by the development of a sufficient portion of secondary flow and the change in the assignment of the main flow to the magnetic field.
- Sudden change of the channel cross sectional area (constriction or widening) accompanied by the development of secondary flow and possibly whirl detachment.
- Magnetic field end effects with inflow and outflow towards the homogeneous magnetic field zone.

The destabilizations of MHD flow resulting from these disturbances will mostly be reflected in a noticeable deformation of the velocity profile. Flow zones near the Hartmann boundary layer and normal to \vec{B} will be more accelerated so that a so-called M-shaped velocity profile might establish. Such M-shaped velocity profiles were detected already in the experiment at low magnetic flux densities for the three types of disturbances mentioned before. The said effects depend above all on the M/Re ratio.

The following examples of these types of MHD flow destabilization will be treated in this report:

- bend flow,
- sharp edged elbow flow,
- flow in the magnetic boundary field

4.3 Bend Flow

Bocheninskii et al [12] investigated the velocity profile at the summit of a bend with an angle of turn of 180° passed by a mercury flow. The bending plane runs in the x-y-direction. The magnetic field occurs in this direction and perpendicular to the straight pipe sections. The left hand part of Fig. 9 shows the velocity profile in the z-direction, the right hand part the velocity profile in the y-direction. The Hartmann numbers are 300 and 0, the Reynolds number is 22750. In the z-direction, i.e., normal to B , the M-shaped deformation of the velocity profile becomes clearly visible at $M = 300$. This deformation does not appear in the y-direction.

4.4 Elbow Flow

Figure 10 shows in a model the flow passing through an elbow [13] in a homogeneous magnetic field with clear destabilization near the inner elbow edge accompanied by a

shear layer S. The flow towards the elbow is normal to the homogeneous magnetic field, the flow away from it is parallel to B_0 .

4.5 Flow in the Magnetic Boundary Field

When a liquid metal flow in a rectangular channel enters a magnetic field zone (Fig. 11a) an eddy current normal to the magnetic field develops in the zone of field augmentation. On account of this eddy current the field of volume forces is distorted which leads to a reduction in core velocity and to an increase in peripheral velocity. This effect of M-type deformation of the velocity profile appears once more at the end of the magnetic field zone.

Figure 11b shows this M-type velocity deformation. Whilst in the diagram on the left hand side this deformation does not occur in the direction of the magnetic field on the y-u-plane, it is clearly evident in the diagram on the right hand side, on the z-u-plane, i.e., normal to B. In the table on the bottom of Fig. 11 [6] the Re- and N-values related to the velocity profiles are indicated. Already plot 3 shows a clear increase in velocity beyond the core flow which develops with growing N into a pronounced velocity maximum getting displaced towards the wall.

5. Corrosion and Heat Transfer in the Magnetic Field

5.1 Corrosion in the Magnetic Field

According to Heitz [14] three single steps must be considered:

- feed of the aggressive material,
- reaction at the phase boundary,
- removal of the corrosion products.

The first and third of these single steps are influenced by a strong magnetic field, this influence being exerted via the velocity distribution and the variation in turbulent mass exchange.

When one estimates the corrosion rate the difficulty arises that the velocities of the single steps must be compared with each other. The following cases can be distinguished:

- The phase boundary reaction proceeds slowly as compared with the transport phenomena. In this case the corrosion rate is determined by the reactions taking place at the phase boundary.

- The transport processes are slower than the reaction at the phase boundary. In this case the corrosion rate is controlled by the transport processes.

- The transport processes and the reaction at the phase boundary occur at comparable rates. In this case the transport processes make a contribution.

It has been found in experiments that material corrosion in lithium and lithium-lead flow is greatly influenced by the flow velocity and the heating rate in the liquid metal. These are indications to the effect that the corrosion rate is determined predominantly by material transport in the liquid metal. This material transport can be described by a model provided that the velocity distribution is known. Therefore, the velocity profiles must be studied for concepts also in which the liquid metal does not serve as a coolant but is circulated solely with a view to extract the tritium. Also in this case relatively high velocities normal to the magnetic field occur in the supply and return manifold which leads to a considerable leveling off in the velocity profile and to very high velocity gradients at the wall.

On account of the large range of parameters to be investigated and the long service lives required for corrosion tests, studying the influence of a magnetic field on liquid metal corrosion may involve a combination of model development and few integral experiments for model verification. It is the task of the experimental work on MHD effects to determine the velocity profiles in the flow cross sections to be investigated. Moreover, an experimental program for studying the influence of a strong magnetic field on liquid metal corrosion could be designed to pursue four goals:

- Investigation of lithium diffusion, possibly also lead diffusion, into the matrix and the grain boundaries of the channel wall using secondary ion and mass spectroscopy.
- With the help of this same method it should be possible to obtain data about the corrosion at the wall surface through liquid metal contact.
- The matrix material dissolved in the liquid metal would have to be investigated by atomic absorption analysis.
- To investigate the deposits specimens can be placed in a colder section of the test loop. These deposits are investigated using the methods of chemical-physical surface analysis (SIMS, AES etc. [15]).

5.2 Heat Transfer in the Magnetic Field

The heat transfer in liquid metal flow is described as follows according to Lyon [16] and Martinelli [17] ($Pe = Re \times Pr$):

$$Nu = C + a * Pe^b \quad (32)$$

C being determined by the thermal conductivity and $a^* Pe^b$ by the turbulent momentum exchange with the pipe wall. In case of sodium flow the semi-empirical relation

$$Nu = 7.0 + 0.025 \times Pe^{0.8} \quad (33)$$

is sometimes used.

In case of liquid metal flow in the magnetic field the turbulence is suppressed with increasing field strength which gives rise to lamination and hence reduces the influence of the Peclet term. The Nusselt-Peclet relation has been assumed to be of the type

$$Nu = C + a^*(Pe^m/M^n) \quad (34)$$

In liquid metal cooled Tokamak reactors Hartmann numbers $M > 10,000$ must be expected. No information is available about the heat transfer for high Hartmann numbers. The constants C , a^* , m and n can be determined in the experiment only.

6. Influence of the Magnetic Field on the Tritium Transport under Conditions of Mixing Convection

The distribution of tritium in the vessel units containing the liquid metal breeding material according to the INTOR concept is determined by the neutron field, on the one hand, and influenced by convection, on the other hand. Convection may be caused by a mixing variable from the temperature field, i.e., free convection and forced circulation for the purpose of external tritium separation (for NET ~ 1 inventory per day). Mixing convection is exposed to the magnetohydrodynamic influence or disturbance from the strong magnetic plasma holding field. It can be globally assumed that the disturbance of the tritium removal from the cylinder units containing the

breeding material is of little importance if it can be guaranteed that the disturbance in tritium distribution is compensated by diffusion. The vessel dimensions are $\sim 1.6 \text{ m} \times 0.26 \text{ m} \times 0.4 \text{ m}$. The breeding material is the eutectic lithium-lead alloy $\text{Li}_{17}\text{Pb}_{83}$. Unfortunately, experimentally determined diffusion coefficients for this alloy are neither available for tritium nor for deuterium or hydrogen. The same applies to pure lead. Only for the lithium-hydrogen system the diffusion coefficients were measured between 700 and 900 $^{\circ}\text{C}$ [18]. If one assumes for the equalization of concentrations by diffusion a mean displacement square $\Delta \bar{x}^2$ of a particle [19] one obtains for its range $\Delta \bar{x}$

$$\sqrt{\Delta \bar{x}^2} = \sqrt{2D \cdot \tau} \quad (35)$$

with D being the diffusion coefficient and τ the duration.

With $D_{\text{H,Li}} = \sim 10^{-7} \text{ cm}^2/\text{s}$ for 400 $^{\circ}\text{C}$ and one day = 86.400 s we obtain as the range

$$\Delta \bar{x} = 0.13 \text{ cm.}$$

Thus, the range of diffusion of the bred tritium particles is very small compared with the cylinder dimensions. Adequate homogenization of the tritium distributed in the cylinder units will not be possible due to the reduced convection in the magnetic field.

Experiments related to the free convection of liquid metal in intense magnetic fields have been possible above all as a result of the classical research work performed by Chandrasekhar [20] and Nakagawa [21]. They have chosen a flat disk with its distinct geometry, i.e., the

diameter of the mercury bath is large compared to the bath height. The heat is supplied from bottom and evacuated on top. To characterize free convection the similarity relations of heat transfer, i.e., the Nusselt, the Grashof and the Prandtl numbers become important. In case of convection in the magnetic field the Chandrasekhar number must be considered in addition:

Nusselt number $Nu = \frac{\alpha \cdot h}{k}$,

Grashof number $Gr = \frac{g \cdot \beta \cdot \Delta T \cdot h^3}{\gamma}$

Prandtl number $Pr = \frac{\gamma}{a^*}$

Rayleigh number $Ra = Gr \cdot Pr = \frac{g \cdot \beta \cdot \Delta T \cdot h^3}{\gamma \cdot k}$

Chandrasekhar number $Q^* = \frac{\sigma \cdot B^2 \cdot h^2}{\rho \cdot \gamma}$

In these characteristic numbers α means the heat transfer coefficient, h means the layer height, k means the thermal conductivity of the liquid metal, g means the acceleration due to gravity, a^* means the thermal diffusivity, ΔT means the thermal gradient, β means the expansion by volume coefficient of the liquid metal, σ means the electrical conductivity of the liquid metal, B means the magnetic flux density, and ρ means the density of the liquid metal.

The Nusselt-Rayleigh relation in the space free of a magnetic field is generally expressed as

$$Nu = a^* \cdot Ra^b \cdot Pr^c \quad . \quad (36)$$

In the magnetic field B , except for the initial zone, a nearly linear dependence of the Rayleigh number on the Chandrasekhar number is observed of

$$Ra = \epsilon \cdot Q^* \quad , \quad (37)$$

where ϵ is a proportionality factor close to 10 (Fig. 12). Then it follows for the Nusselt-Chandrasekhar relation

$$N = a^* \cdot (\epsilon \cdot Q^*)^b \cdot Pr^c \quad , \quad (38)$$

with a^* , b and c being variables to be determined empirically.

An estimate of the Chandrasekhar number for the dimension of the liquid metal containing cylinder according to the INTOR concept at $B = 6$ T gives $Q^* \approx 10^{10}$.

Approximation of the real convective conditions in the breeding material cylinders traversed by cooling channels (Fig. 12) will call for application of comprehensive computer programs such as the 3D thermohydraulics code, COMMIX 1A [22]. An extension to include the influence of the magnetic field would have to be integrated in this code.

7. Pressure Loading on Components of the First Wall under Conditions of Quick Variations of the Magnetic Field

In the liquid metal blanket pressure pulses might be generated in the liquid metal due to non-steady-state magnetic fields. These transient magnetic fields may develop if the fusion plasma collapses due to instabilities (plasma disruptions). According to Onega et al [23] the disruption times during which the poloidal magnetic field generated by the plasma current drops to zero occur have durations between 0.1 ms and 25 ms. By contrast, the switch off time in normal pulse operation is ≈ 3.3 s.

For a poloidal field strength $B_p = 0.6 \text{ T}$ ($\sim 10\%$ of the toroidal field strength B_T) according to the ORNL Tokamak Blanket Design Study [24] the quick poloidal field variations \dot{B}_p correspond to these disruption times.

	(ms)	\dot{B}_p (T/s)
Normal operation	3.3×10^3	0.18
Least severe disruptions	24	25
Most severe disruptions	10^{-1}	6000

The rather simplified relation between field variation velocity and pressure pulse is evident from

$$\hat{p} = \frac{1}{8} \cdot \sigma \cdot a^2 \cdot B_p \cdot \dot{B}_p \quad (39)$$

where σ is the electrical conductivity of the liquid metal, and a is the radius of the module of the first wall, Fig. 13 (total number: 67,000 modules). The attempt of raw estimating these pressure pulses for the blankets, according to the INTOR 1982 reactor study [25] (Fig. 14), has produced the values entered in the following table. They apply near the first wall

B-field variation \dot{B}_p (T/s)	Pressure Pulse (bar)	
	ORNL 80	INTOR 82
0.18	9.4×10^{-4}	7.2×10^{-2}
25	0.13	10.5
6000	32	2.6×10^3

It appeared that the much larger vessel units under the NET/INTOR blanket design concept with the area of $\approx 1.0 \text{ m} \times 0.26 \text{ m}$ facing the plasma might result in much higher pressure pulses. In the INTOR study [25] the major disruption time between 5 and 20 ms is assumed.

8. Investigations Required

To effectively approach the reality of MHD problems in the blankets of fusion reactors both the field of the magnetic flux density and the experimental space must be chosen of sufficient size. Branover [6] presented a survey of the magnetic field facilities used in order to investigate the MHD flows (Table 3). It is striking that the majority of magnetic fields occur well off the plasma holding fields of fusion reactors. Another deficiency of these facilities consists in the small dimensions of the experimental working space inside the magnet.

Therefore, a larger experimental magnetic field facility (MHD large-scale facility) must be provided. It should be equipped with a superconducting dipole magnet with a magnetic flux density of 5 tesla and a working space in the homogeneous field of 1.0 m x 0.4 m x 0.3 m (Fig. 15) (hot condition). Thus, it should guarantee an adequate margin in the selection of the liquid metal fluid.

The Karlsruhe Nuclear Research Center has accumulated experience over many years in the field of liquid metal studies and magnet development.

At the Institute for Reactor Components (IRB) a normal conducting solenoid magnet of the BITTER type was erected some years ago. These are the technical data [5]:

Central magnetic flux density B	6.5 tesla
Diameter of the experimental space	34 mm
Length of the homogeneity range	60 mm for $\Delta B/B = 3\%$
Dissipated power P at 6.5 T	1.15 MW

The program of studies should contain the following items:

- (a) MHD pressure losses in straight channels (integral pressure measurement).
- (b) MHD pressure losses in channels with change of direction and channel widening (integral and differential pressure measurements).
- (c) MHD velocity profiles.
- (d) Corrosion and mass transport in the magnetic field.
- (e) Heat transfer in the magnetic field.
- (f) Convective flow in the magnetic field.
- (g) Pressure pulses in the non-steady-state magnetic field.

The MHD large-scale facility is an indispensable necessity for implementation of the global program (a through g) with great Hartmann number (>8000).

The study of bend flow (b) with an angle of turn of 180° without and with channel wall conduction up to Hartmann numbers of 1500 as well as investigations of orientation into pressure pulses in non-steady-state B-fields can be performed in the BITTER type magnet installed at the IRB.

Literature

- /1/ Hartmann, J.: "Hy-Dynamics I", Det. Kgl. Danske Videnskabernes Selskab., Mathematisk-Fysiske Meddelelser XV, 6 (1937) p. 2.
- /2/ Hoffman, M.A.; Carlson, G.A.: "Calculation Technique for Estimating the Pressures Losses for Conducting Fluid Flows in Magnetic Fields". UCRL 51010, (Febr. 1971).
- /3/ Hunt, J.C.R. and Hancox, R.: "The Use of Liquid Lithium as Coolant on a Toroidal Fusion Reactor, Pt. I, Calculation of Pumping Power" CLM-R 115, 1971.
- /4/ Lielausis, O.: "Liquid-Metal Magnetohydrodynamics". Atomic Energy Review 13 (1975) pp. 527-581.
- /5/ Branover, H.: "Resistance of Magnetohydrodynamic Channels". Magnetohydrodynamics V. 3 No. 4 (1967) pp. 3-16.
- /6/ Branover, H.: "Magnetohydrodynamic Flow in Ducts". Jerusalem 1978.
- /7/ Carre, F.; Proust, E.; Remoleur, E.; Rocabay, A. and Tilliette, Z.: "Fusion Reactor Blanket Comparative Evaluation Study". Rapport EMT/SERMA/BP 84 IN 584 "T" 3591-21-000, /18/1/84/.
- /8/ Hancox, R. and Booth, J.A.: "The Use of Liquid Lithium as Coolant in a Toroidal Fusion Reactor, Pt. II, Stress Limitations". CLM-R 116, 1971.
- /9/ Michael, I.: "Experimental Investigation into the MHD Pressure Drop across Meander Shaped Channels", Third Seminar on MHD-Flow and Turbulence, BEER-SHEVA (March 1981).
- /10/ Abdou, M. et al.: "Blanket Comparison and Selection Study". ANL/FFP-83-1, Vol. I 1983, Chapter VII.

- /11/ Stephan, K.: "Strömungswiderstand und Endwerte der Wärmeübergangskoeffizienten bei ausgebildeter magnetohydrodynamischer Rohrströmung". Wärme- und Stoffübertragung 4 (1971) pp. 32-38.
- /12/ Bocheninskii, V.P.; Tananaev, A.V.; Yakovlev, V.V.: "Experimental Investigation of the Flow of an Electrically Conducting Liquid in Curved Tubes of Circular Cross Section in an Intense Magnetic Field" Magnetohydrodynamic, Vol. 13, No. 4 (1977) pp. 431-435.
- /13/ Holroyd, R.J. and Hunt, J.C.R.: "Workshop on Liquid Metal MHD in Fusion". Argonne National Laboratory, August 9-11, 1983.
- /14/ Heitz, E.: "Untersuchungen von Transportvorgängen bei der Korrosion". Werkstoff und Korrosion (1964) H.1. pp. 63-67.
- /15/ Michael, I.; Plog, C.: "Dünnschichtenanalyse von Druckwasserkorrosionsschichten auf INCOLOY 800-Proben". Metall, 31. Jahrgang, Heft 3, March 1977, pp. 252-256.
- /16/ Lyon, R.N.: "Liquid Metal Heat-Transfer Coefficients". Chemical Engineering, V. 47 (1951) No. 2, pp. 75-79.
- /17/ Martinelli, R.C.: "Heat Transfer to Molten Metals". Transactions ASME, V. 69 (1947) 947.
- /18/ Alire, R.M.: "Transport of Hydrogen in Liquid Lithium". Journal of Chemical Physics V. 65 (1976) No. 3, pp. 1134-1137.
- /19/ Einstein, A.: "Über die von der molekularkinetischen Theorie der Wärme geforderte Bewegung von in ruhenden Flüssigkeiten suspendierten Teilchen". Annalen der Physik 4. Folge, Bd. 17 (1905), pp. 549-560.
- /20/ Chandrasekhar, S.: "Hydrodynamic and Hydromagnetic Stability". Oxford University Press, 1981.

- /21/ Nakegawa: "Experiments on the Inhibition of Thermal Convection by a Magnetic Field". Proc. Royal Society London, V. 240 (1957) 108-113.

- /22/ Baumann, W.; Willerding, G.: "Eingabebeschiebung und Benutzeranleitung für den amerikanischen 3-D-Thermohydraulik-Code COMMIX-1A". Unveröffentlicher Bericht 1983.

- /23/ Onega, R.J.: "Major Plasma Disruptions in TNS", ORNL/TM6616 Oak Ridge National Laboratory (February 1979).

- /24/ N.N.: "Tokamak Blanket Design Study - Final Report". ORNL/TM-7049, August 1980.

- /25/ N.N.: "INTOR - International Tokamak Reactor Phase II A Workshop, Vol. III, EUR FU BRU". December 1982 Brussels.

- /26/ Maurer, W.: "Entwicklungen auf dem Gebiet der Hochstrom-Supraleitung im Kernforschungszentrum Karlsruhe; KfK-Bericht 2290, May 1970.

- /27/ Shercliff, J.A.: "Magnetohydrodynamic, Pipe Flow, Pt. 2. High Hartmann Number". J. Fluid Mechanics 13 (1962), 573.

- /28/ Chang, C.C. and Lundgren, T.S.: "Duct Flow in Magnetohydrodynamics". Z. Math. Phys. 12 (1961), 100.

- /29/ Dunn, P.F.: "Single-Phase and Two-Phase Magnetohydrodynamic Pipe Flow". J. Heat Transfer V. 23 (1980), 373-385.

Table 1: Admissible Load in MPa of some Materials without and with Irradiation at 500 °C [7]

Material	Admissible Load (MPa)		
	Without Irradiation 5 x 10 ⁴ h	With Irradiation 100 dpa	200 dpa
PCA 316 SS (Ti) 25% cold worked	205	150	-
HT-9 HT-9 91334 XXA3587	140 (105 h)	163	125 (150 dpa)
V-15Cr-5Ti	220	165	105

Table 2a: Friction Coefficients for MHD Flow (Lielausis 1975).

LIQUID-METAL MHD FLOW CONFIGURATIONS AND EXPRESSIONS ASSOCIATED WITH PRESSURE DROP

$Re = \frac{\rho v \ell}{\eta}$; $Ha = B \ell \sqrt{\frac{\sigma}{\eta}}$; $N = Ha^2 / Re = \frac{\sigma B^2 \ell}{\rho v}$	$\lambda = dp/dx \cdot 2 \ell / \rho v^2$; $\zeta = 2 \Delta p / \rho v^2$; $C = 2 F_X / \rho v^2$	ℓ - charact. length = \bigcirc ρ - density η - viscosity σ - conductivity v - mean velocity B - magn. flux density
---	--	---

	Flow configuration	Turbulent	Laminar
1		$\lambda = \lambda_0 (1 + 1.95N)$ $Re \geq 3 \times 10^4$	$\lambda = 2Ha/Re$ $Ha \geq 7$
2		$\lambda = \lambda_0 (1 - 3.85N)$	$\lambda = \frac{2Ha}{Re} \left(1 - \frac{0.852}{Ha \sqrt{2} B} \right)^{-1}$
3		$\lambda = \lambda_0 (1 + 1.67N)$ $B = 2$	
4		$\lambda = \lambda_0 (1 - 2.8N)$	
5			
6			$\lambda = \frac{2Ha}{(1+\alpha)Re} (\alpha Ha + 1)$ $Ha \geq 7; \alpha = \frac{\sigma_1 \delta}{\sigma a}$
7			$\lambda = \frac{\pi Ha}{(1+\alpha)Re} \left[\frac{\pi}{2\alpha H} - \frac{1}{(\alpha Ha^2 + \dots)} \right]$
8		$\lambda = 2N;$	$\alpha Ha \gg 1; \alpha \gg 1;$
9			$\lambda = \frac{2}{Re} \left[\frac{Ha^2 th Ha}{Ha - th Ha} - 3 + P\left(0; \frac{a}{b}\right) + \frac{\alpha Ha^2}{1 + \alpha} \right]$

Table 2b: continued

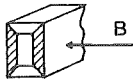
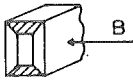
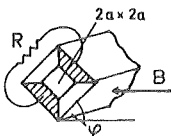
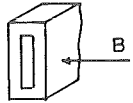
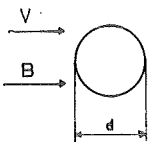
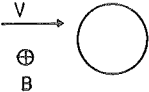
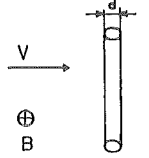
	Flow configuration	Turbulent	Laminar
10		$\lambda = \lambda_0 \left[1 - 1.85 \left(\frac{Ha}{Re} \right)^{1.6} \right]$ (f)	$\lambda = 16/Re$ (f)
11		$\lambda = 33\lambda_0 (1 + 2N)$ $\beta = 1; N \geq 0.3;$	$\lambda = \frac{2}{Re} [0.3/\beta Ha^{3/2} + 1/Ha^2]^{-1}$ (a)
12		$\lambda = \lambda_0 (1 + 2N)$	$\lambda = \frac{2Ha}{Re} \left[1 - \frac{0.956}{\beta Ha^{1/2}} - 1/Ha - O(1/Ha^{3/2}) \right]^{-1}$ (a)
13		$\lambda = \frac{33\lambda_0}{\text{ch} 2\varphi} (1 + 2N)$ $\varphi < 45^\circ; R = \infty$	$\lambda = \frac{N}{4} \left[\sec^2 \theta \left(1 - \frac{1}{Ha \cos \theta} \right) \right]^{-1}$ (a) $\theta = \pi/2 - \varphi; \varphi \leq 45^\circ; R = 0;$
		$\lambda = 133\lambda_0 (1 - \text{th} 2\varphi) \times (1 + 2N)$ $\varphi > 45^\circ; R = \infty$	$\lambda = \frac{N}{4} (1 + \tan \theta)^{-1}$ (a) $\theta = \frac{\pi}{2} - \varphi; 45^\circ \leq \varphi < 90^\circ; R = 0$
14			$\lambda = \lambda_0 (1 + \gamma N)$ $2 \leq \gamma \leq 6$ (a)
15		$C = 0.33 Ha/\sqrt{Re}$ $10^4 \leq Re \leq 2.5 \times 10^5;$ $10 \leq N \leq 80$	$C = C_0 (1 + 3/8 Ha)$ $Re \lesssim 1; Ha \ll 1;$ $C = C_0 + 2/q Ha$ $Re < cHa; Ha \gg 1;$ (d)
16		$C = C_0 (1 + Ha/\sqrt{Re})$ $10^3 \leq Re \leq 8.6 \times 10^3; 0 \leq N \leq 1.5$ $C = C_0 (1 + 0.7 Ha/\sqrt{Re})$ $2 \times 10 \leq Re \leq 5 \times 10^2;$ $0 \leq N \leq 2.3 \times 10^3$	$C = C_0 (1 + 9/16 Ha)$ $Re \ll 1; Ha \ll 1;$ (d)
17		$C = C_0 (1 + 2.2 Ha/\sqrt{Re})$ $l/d \approx 30$	$C = \frac{16\pi}{Re} \frac{1}{2kn4/Ha-2.16}$ $Re \ll 1; Ha \ll 1;$ (d)

Table 2c: continued

	Flow configuration	Turbulent	Laminar				
18				$\zeta \approx 0.2N$	(b)		
19				$\zeta = \zeta_0 + 11.2N \left(1 - \frac{a_1}{a_2}\right)$ ($a_2/a_1 \geq 2.5$)	$\left(\frac{a_2}{2}\right)$		
20				$\zeta = \zeta_0 + 0.74N \left(1 - \frac{d^2}{D^2}\right)$	(D)		
21				$\zeta = \zeta_0$; $\zeta = \zeta_0 (1 - 0.38N)$; $\zeta = \zeta_0 (1 - 0.86N)$;	$\frac{a_2}{a_1} \geq 6$ $= 2.5$ $= 1.67$	$\left(\frac{a_2}{2}\right)$	
22				$\zeta = \zeta_0 + \frac{0.15(\omega-1)}{\omega} N$; $\zeta = \zeta_0 + \frac{(0.5 - 0.7\omega^{-1})(\omega-1)}{\omega} N$	$\omega = \frac{D^2}{d^2} \leq 2$ > 2	(D)	
23				$\zeta = \zeta_0 + kN$; $\zeta = \zeta_0 + (1.4 - m) kN^{1-m}$;	$N \leq (1.4 - m)^{1/m}$; $N > (1.4 - m)^{1/m}$;	$k = f_1 \left(\frac{kD}{d}; \frac{D}{d}; n\right)$; $m = f_2 \left(\frac{kD}{d}; \frac{k_d}{d}\right)$;	(d)
24				$\lambda = \lambda_0 + kN$	$k = 1 - \frac{I_1(\beta)}{\beta I_0(\beta) - I_1(\beta)}$; $\beta = 2\pi R/T$;	(2R)	
25				$\lambda = \lambda_0 + kN$	$k = 1 - 1/\beta \text{ th } \beta$; $\beta = 2\pi b/T$;	(2a)	

Table 3: MHD Experimental Facilities*

Experimenter	Size of Magnet (mm)	Air Gap in Magnet (mm)	B _{max} (Tesla)	Remarks
Hartmann and Lazarus (1937)	16.7 x 360	3	1.2	Uncooled
Murgatroyd (1953)	127 x 305	25.4	1.53	"
Lykoudis (1965)	305 x 1270	76	1.5	Water cooled
Physics Inst. Latv. Acad. Sci (Branover.1967 (1))	70 x 380	15	2.0	Uncooled
Lecocq (1964)	120 x 600	60	1.5	Water cooled
Ben Gurion University, Beersheva, Israel (Branover and Gershon, 1976 (1))	100 x 800	40	0.75	"
Moreau (1963)	200 x 560	60	1.0	"
Globe (1961)	Solenoid L = 450	ø38	0.57	"
Kovner, Krasil'nikov and Nironov (1965)	Solenoid L = 1200	ø50	0.75	"
Genin and Zhilin (1966)	Solenoid L = 706	ø38	1.1	"
Klebanoff and McMichael (1976)	Solenoid L = 975	ø178	0.7	"
Oak Ridge (Young, Holcomb, Fraas, 1975)**	Solenoid L = 1170	ø292	4.0	"
KfK-IRB (Michael, 1979)**	Solenoid L = 145	ø35	6.5	"
Branover, 1978*, (supplemented)**				

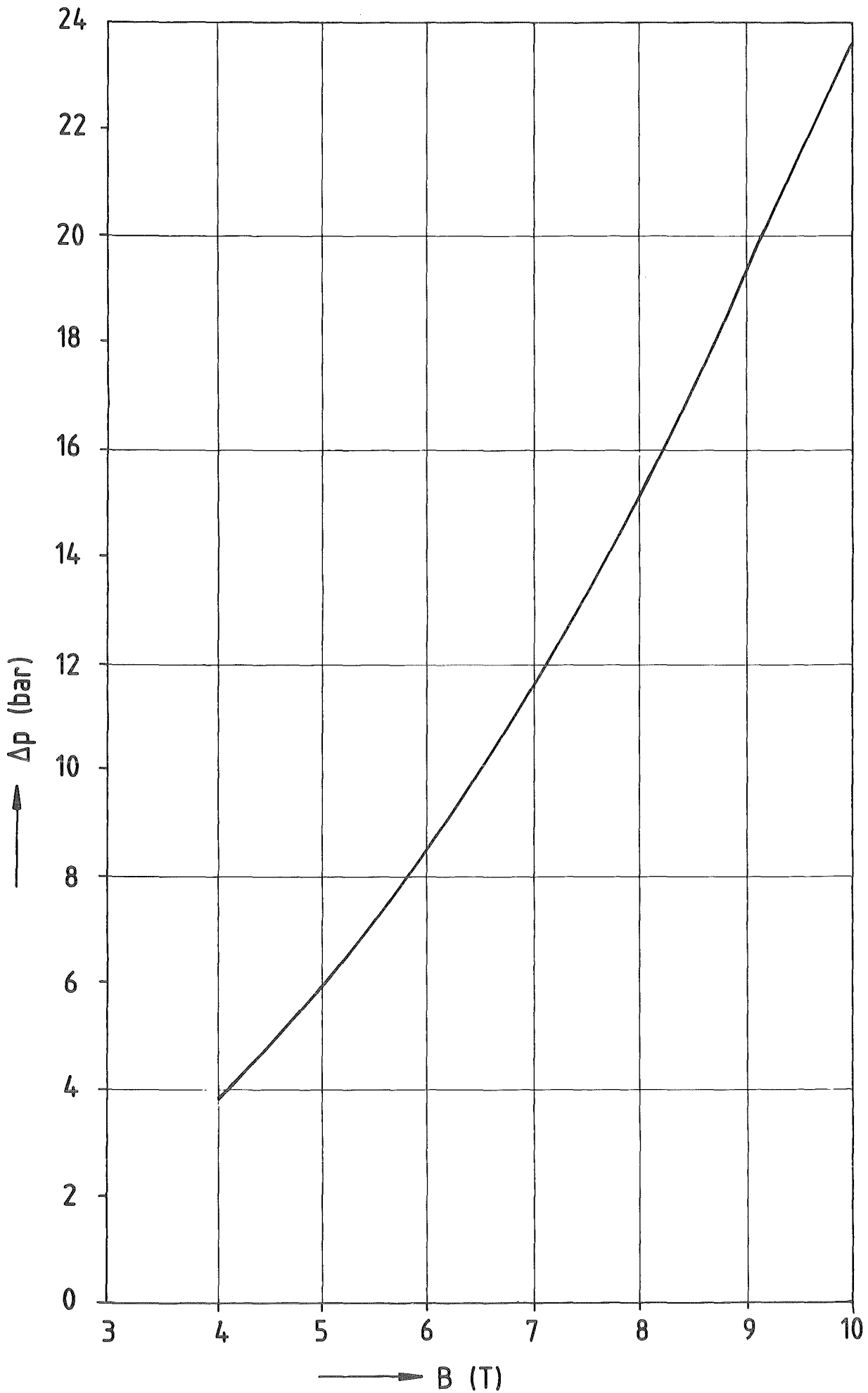


Fig. 1: MHD pressure loss Δp in a lithium supply manifold as a function of the magnetic field B .

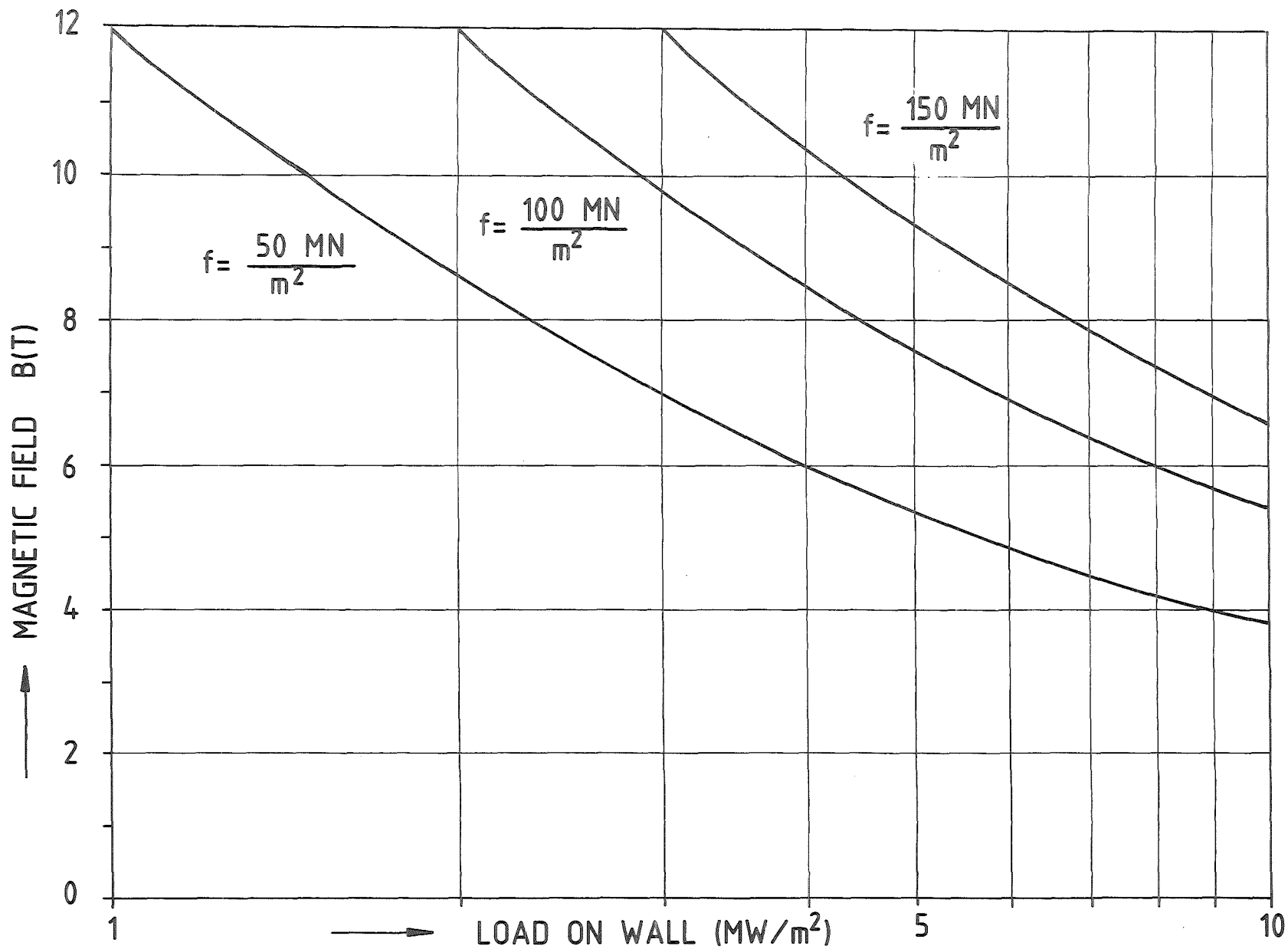
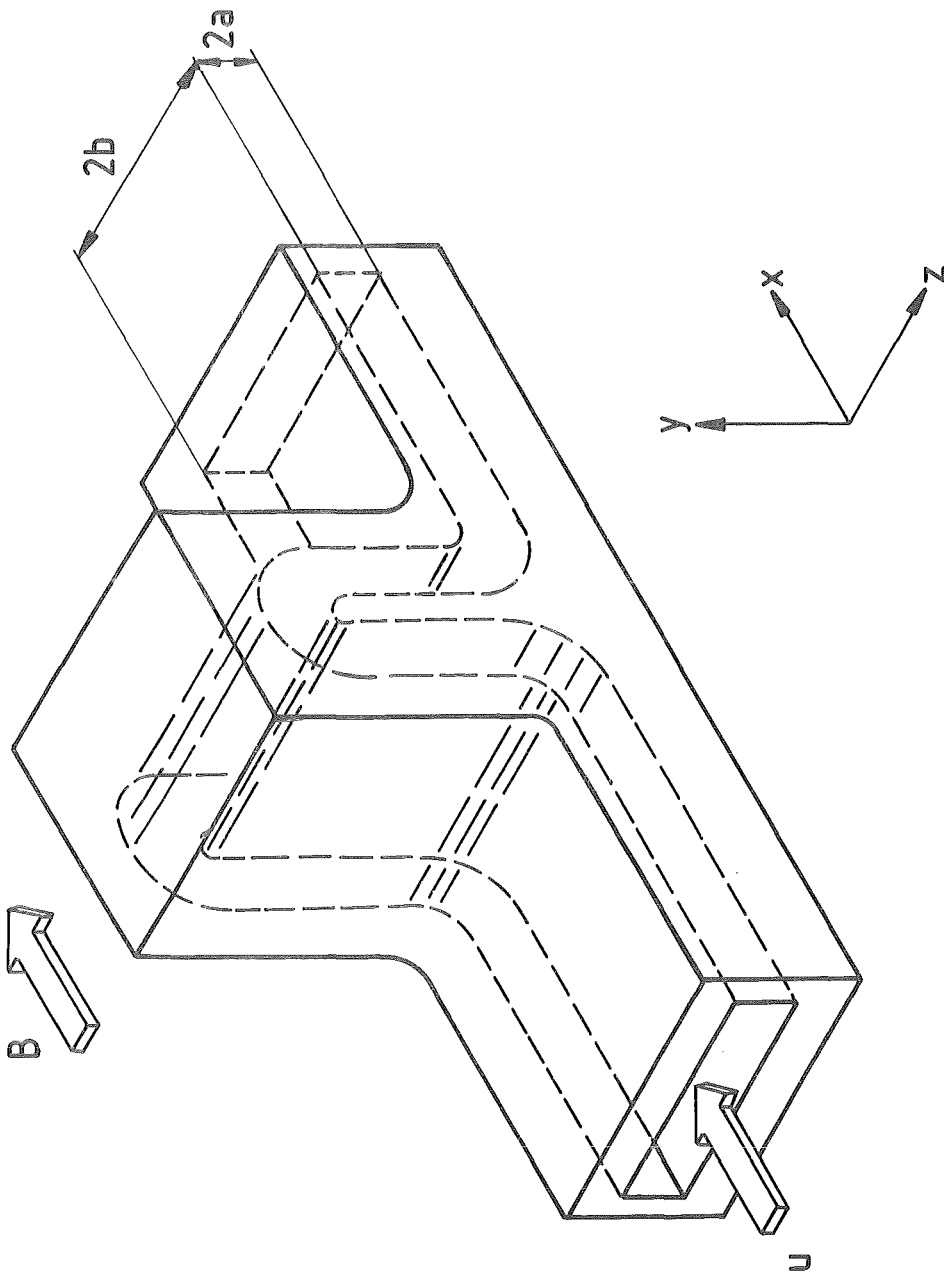
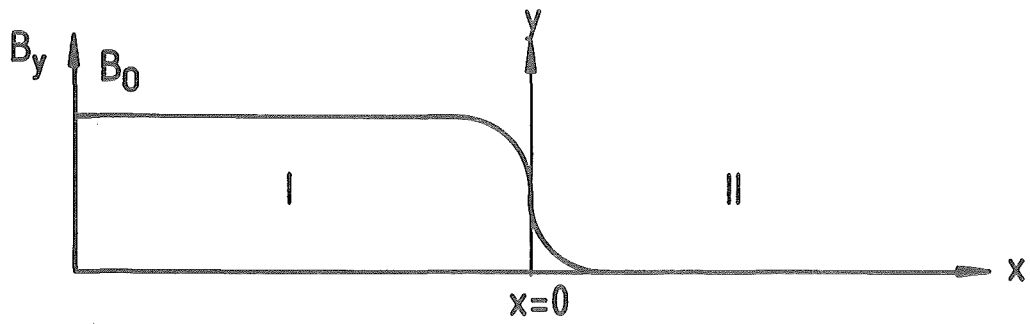


Fig. 2: Limited wall load in MW/m² and magnetic field B as a result of stress f in the wall.



KJK

Fig. 3: Schematic representation of the MHD test channel .



DEVELOPMENT OF B-FIELD

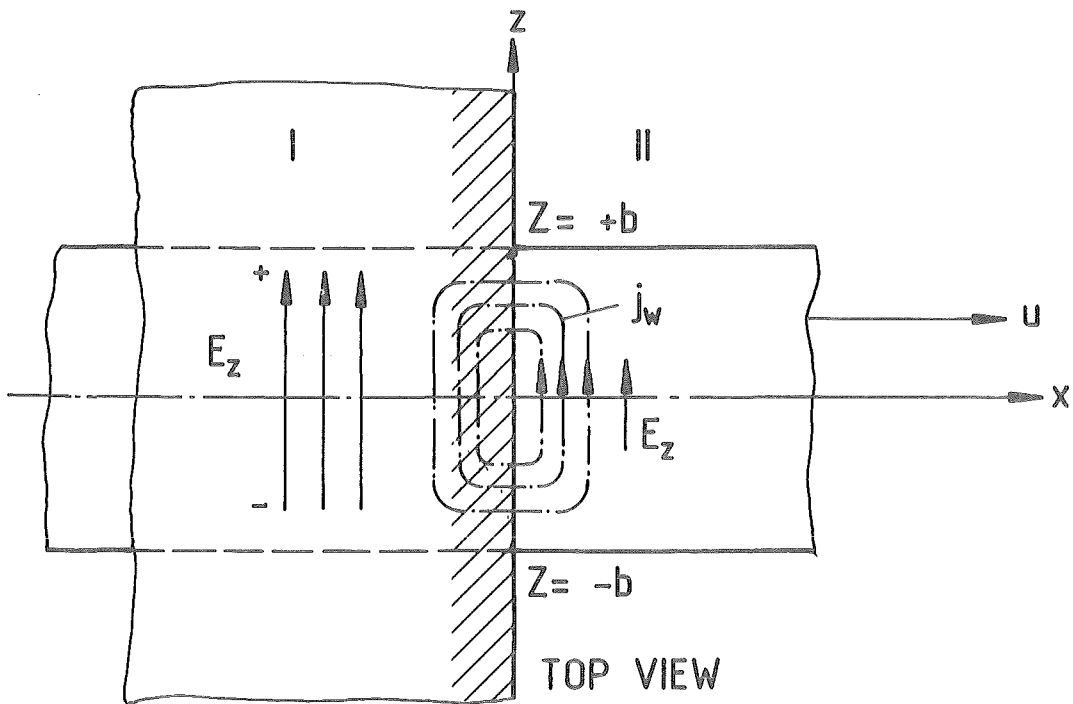
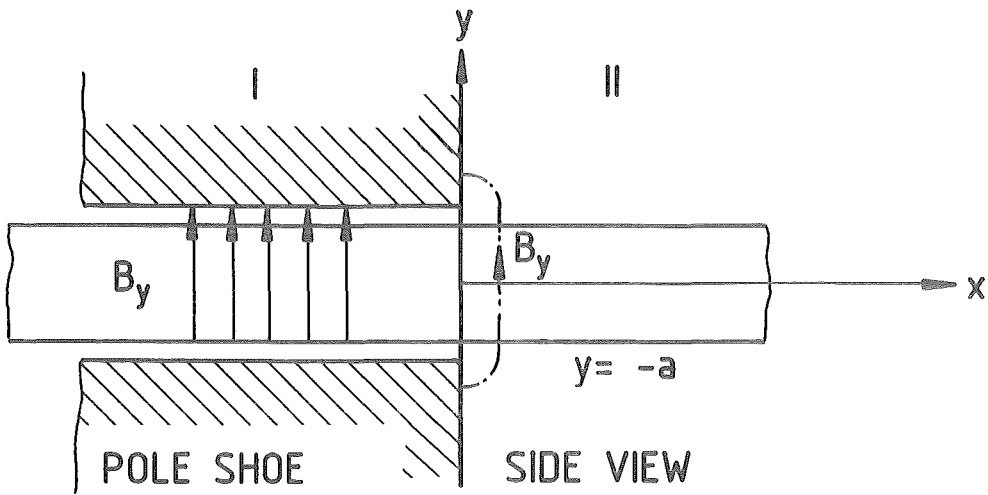


Fig. 4: MHD-Model

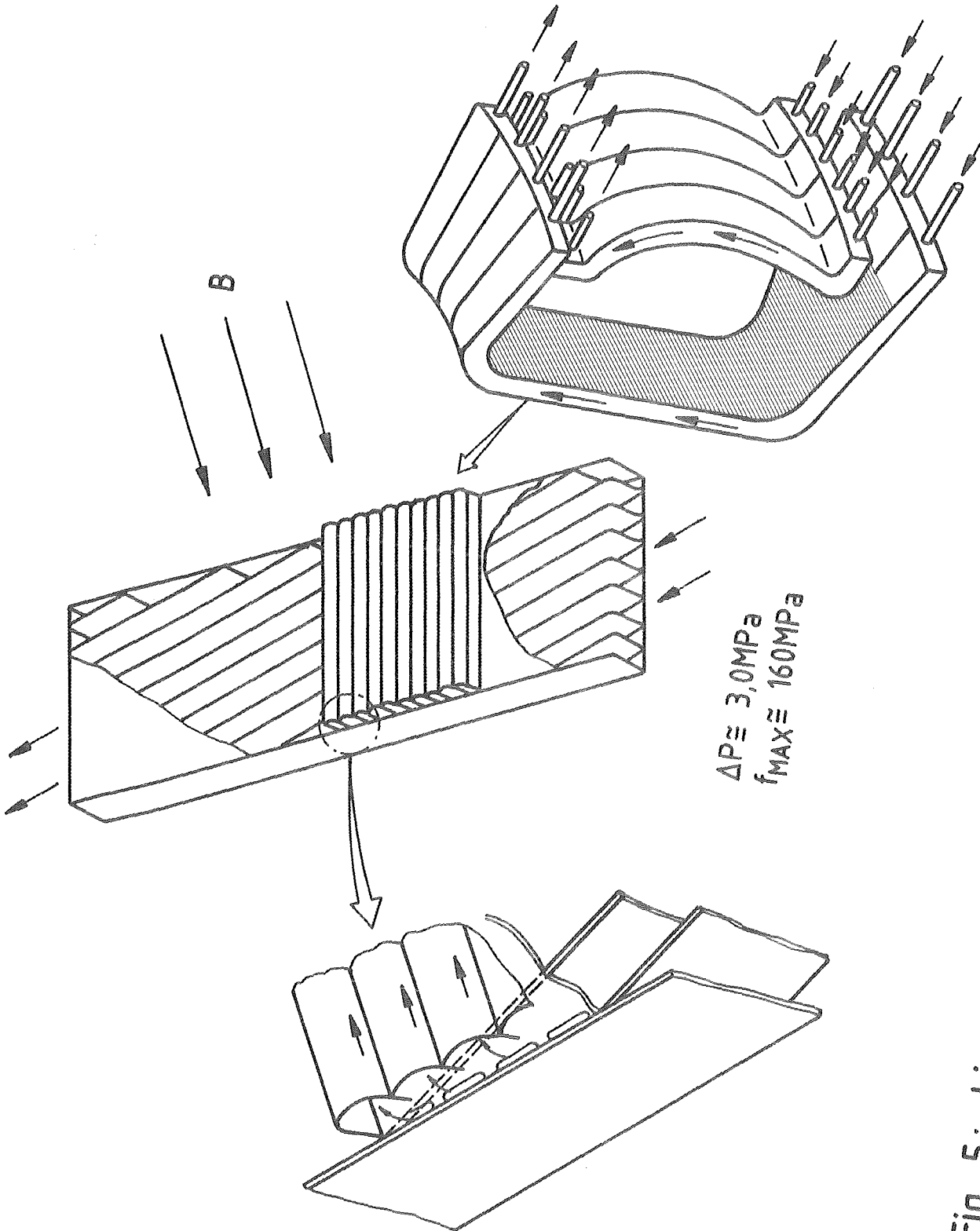


Fig. 5: Liquid metal flow concept proposed by ANL.

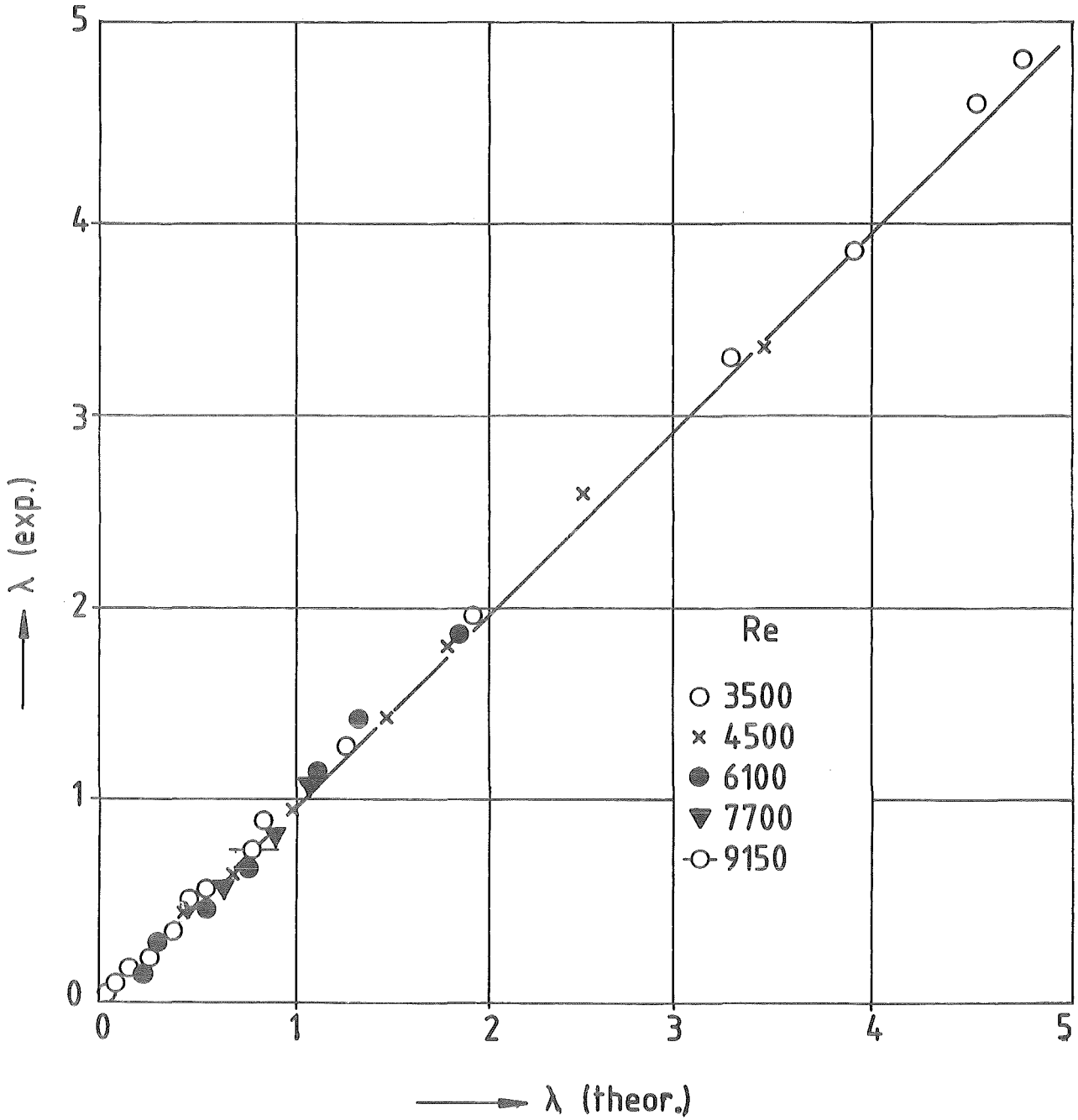


Fig. 6: Comparison of experimental and theoretical friction coefficients of MHD pipe flow and wall conduction (Branover 1967)

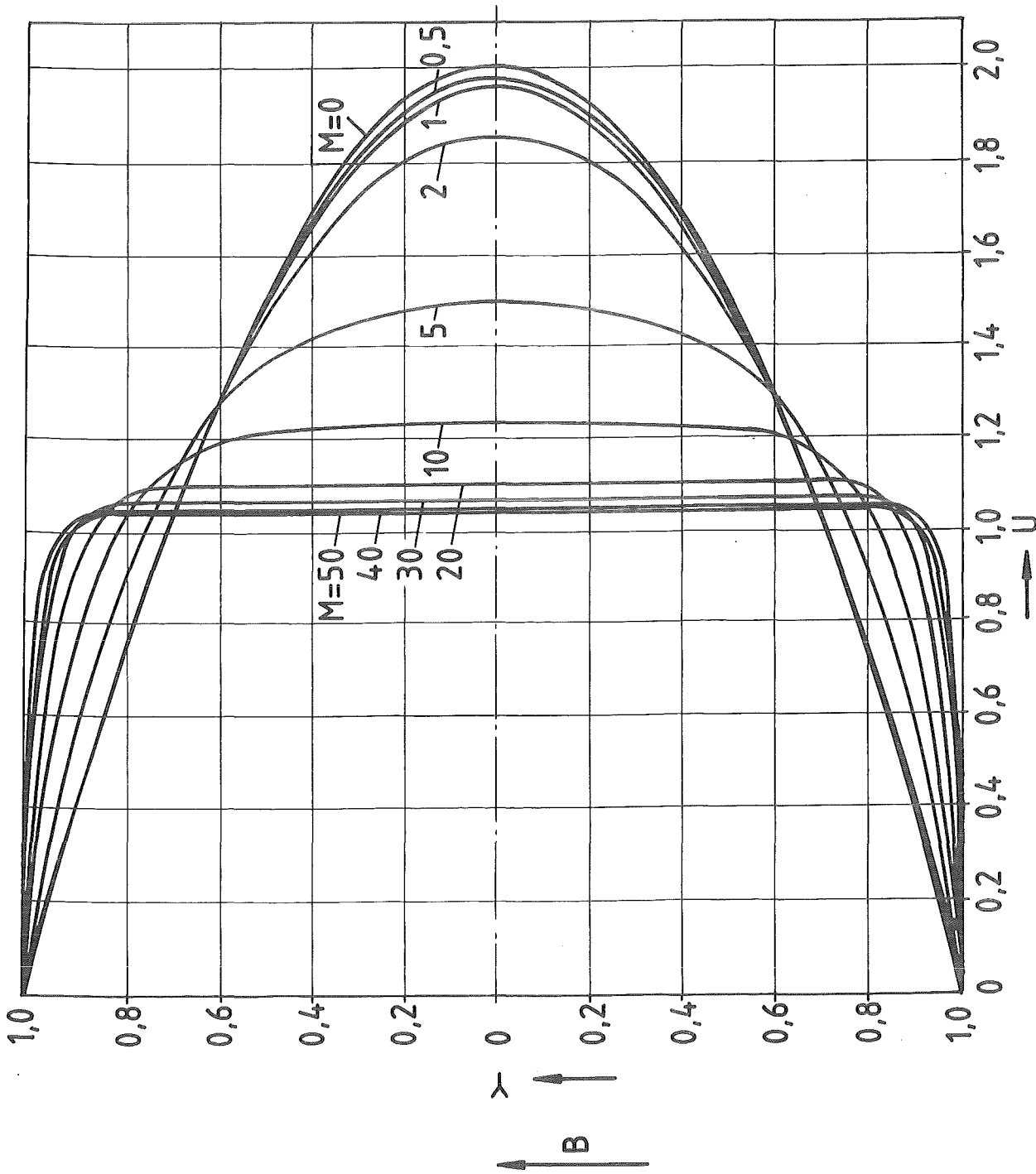


Fig. 7: Velocity profiles :
 Y = dimensionless profiles
 U = dimensionless velocity
 M = Hartmann number

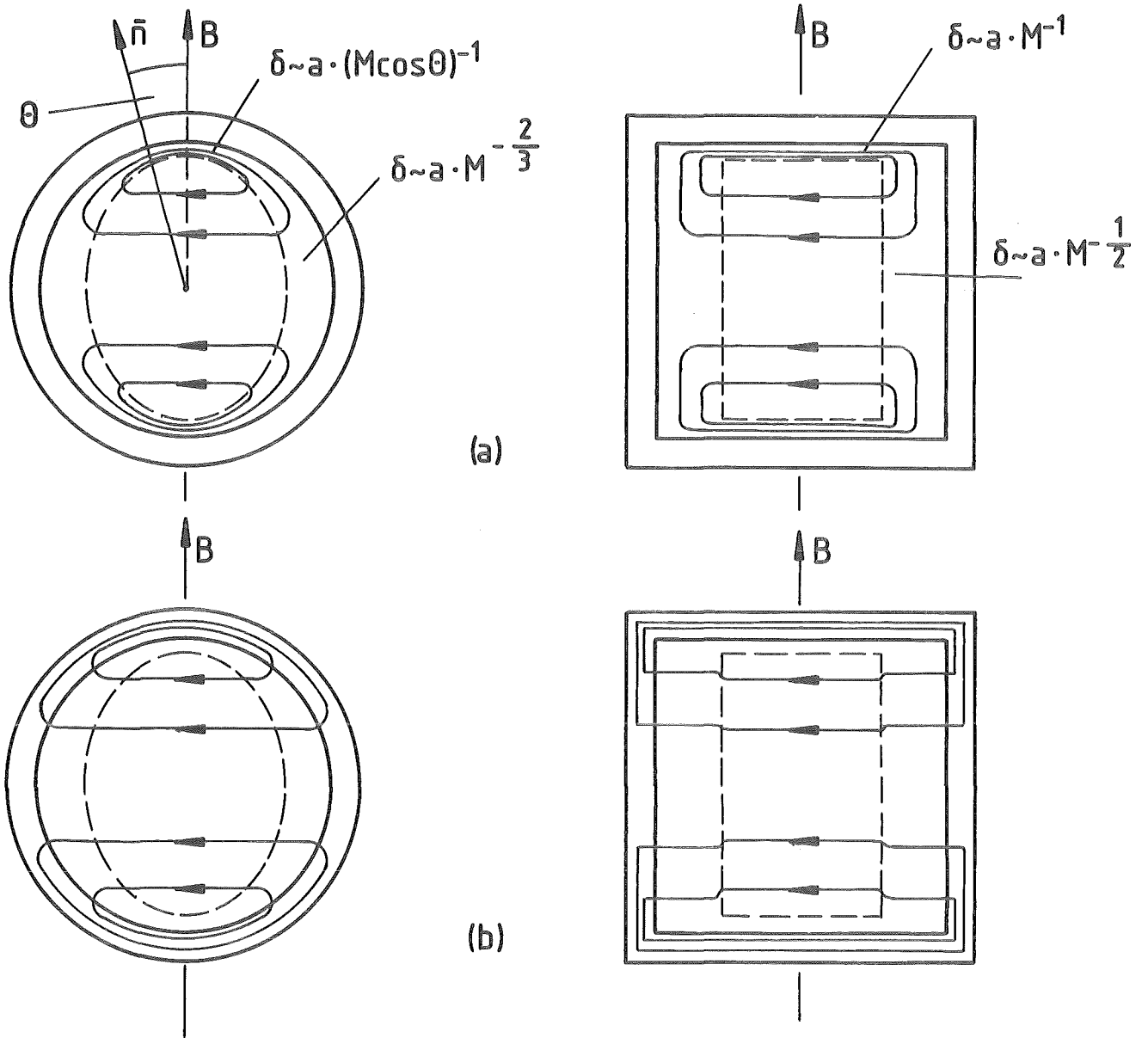


Fig. 8: Electric current paths in channels within an intense magnetic field.
 a) Non-conducting channel wall;
 b) highly conducting channel wall.
 Hartmann boundary layers $\delta \sim a \cdot M^{-m}$

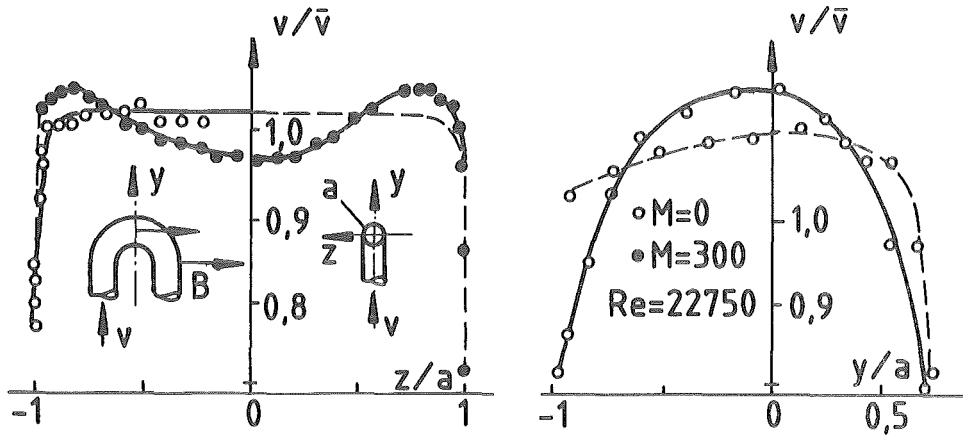


Fig. 9: Velocity profile of bend flow with an angle of turn of 180° on the xz -plane (left) and xy -plane (right) (Bocheninski et al. 1977)

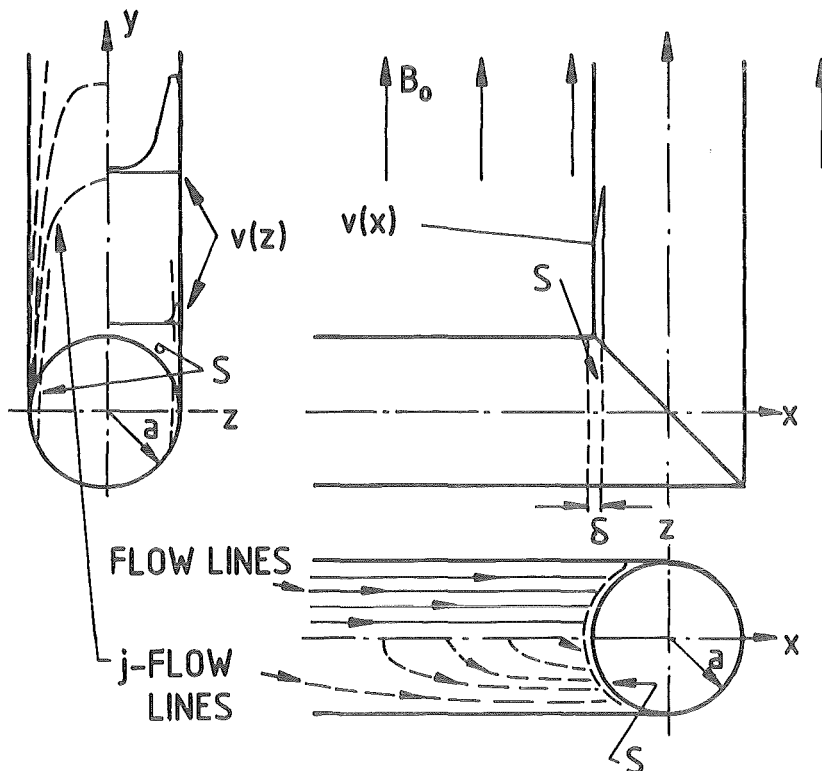


Fig. 10: Model of MHD elbow flow S = shear layer
 δ = thickness of S

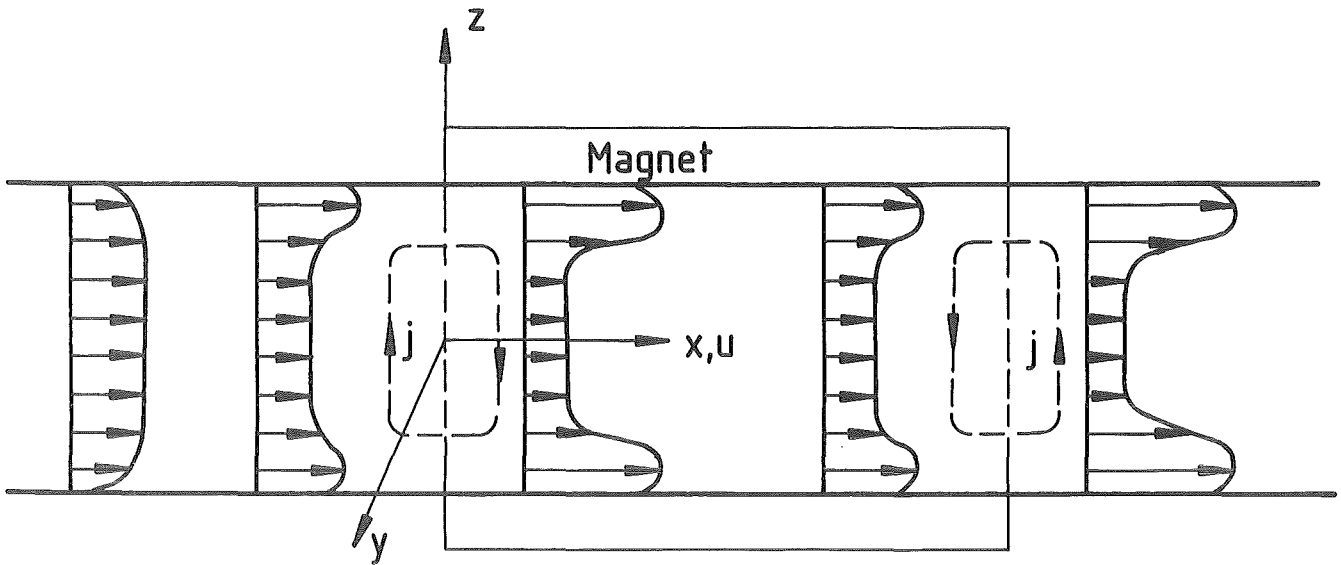


Fig. 11a: Schematic representation of M-shaped velocity distribution due to B-boundary effects.

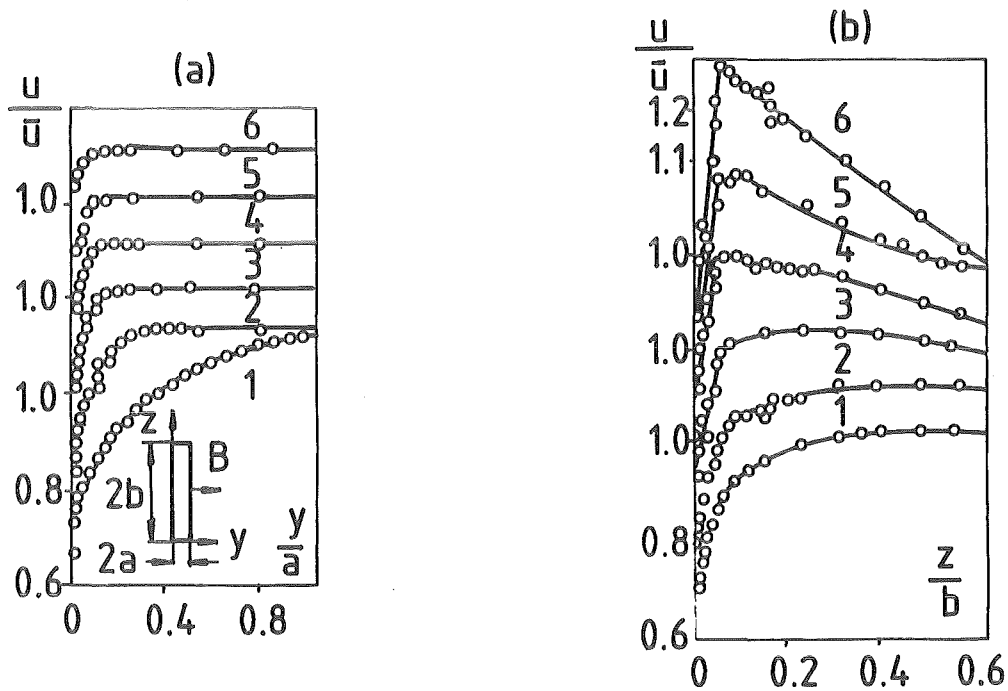


Fig. 11b: Velocity distribution $\frac{u}{\bar{u}}$ in the B-boundary field
 a) on the x-y plane, b) on the x-z plane.

	1	2	3	4	5	6
N	0	0.256	0.713	1.4	1.8	2.45
Re	$3.5 \cdot 10^5$	$3.5 \cdot 10^5$	$3.5 \cdot 10^5$	$3.5 \cdot 10^5$	$20 \cdot 10^5$	$20 \cdot 10^5$

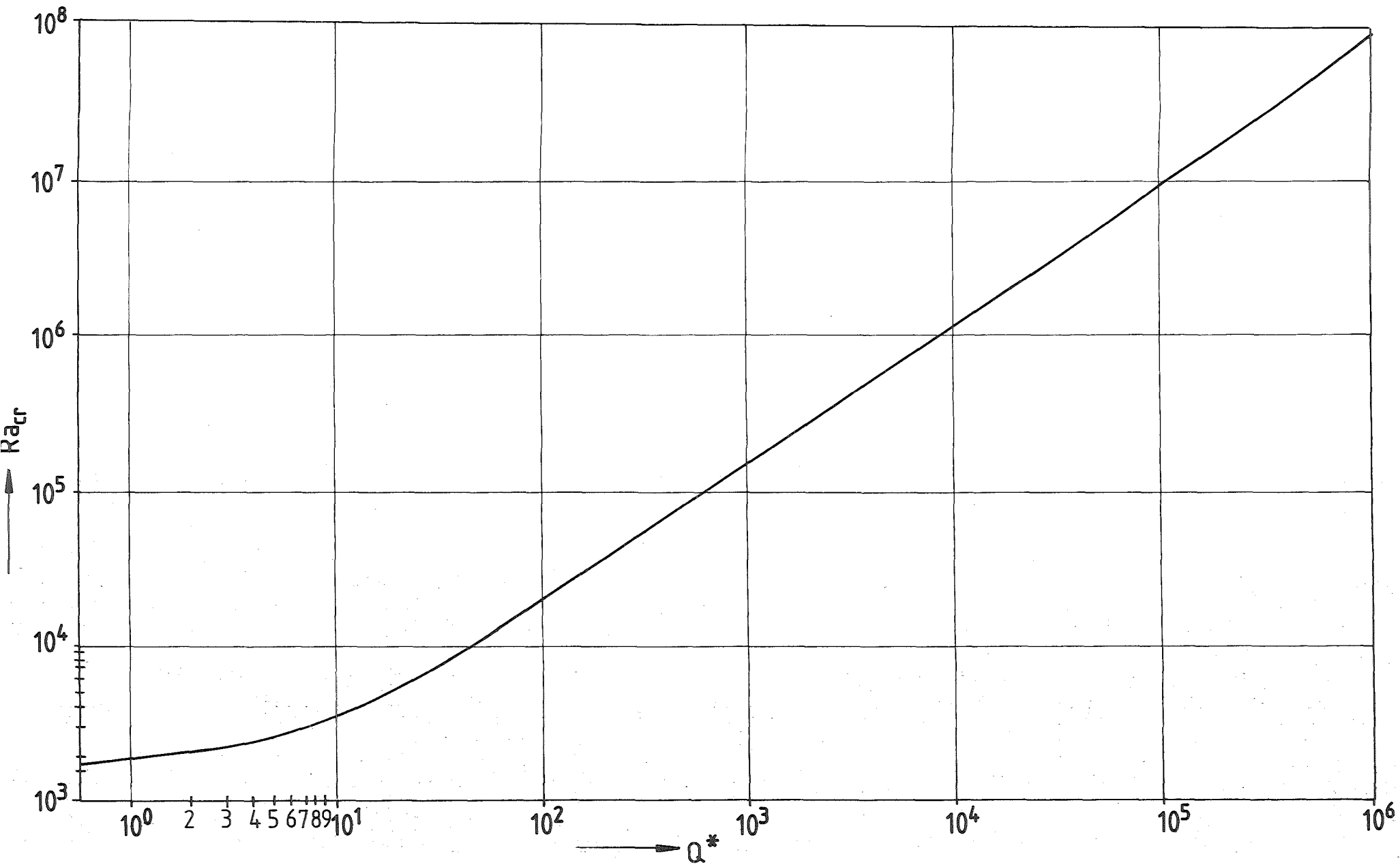


Fig. 12: Critical Rayleigh number Ra_{cr} versus Chandrasekhar number Q^* (Chandrasekhar 1953)

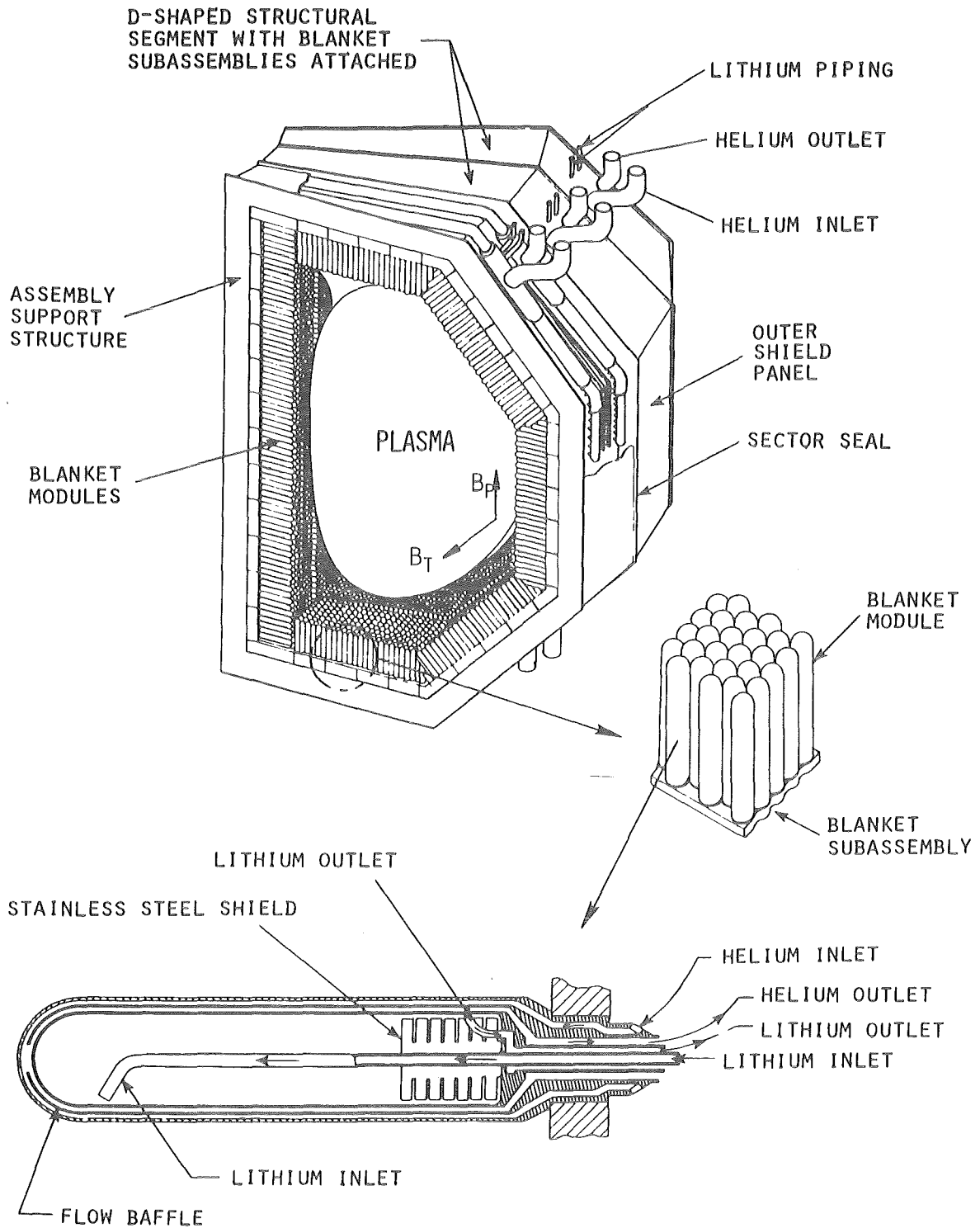
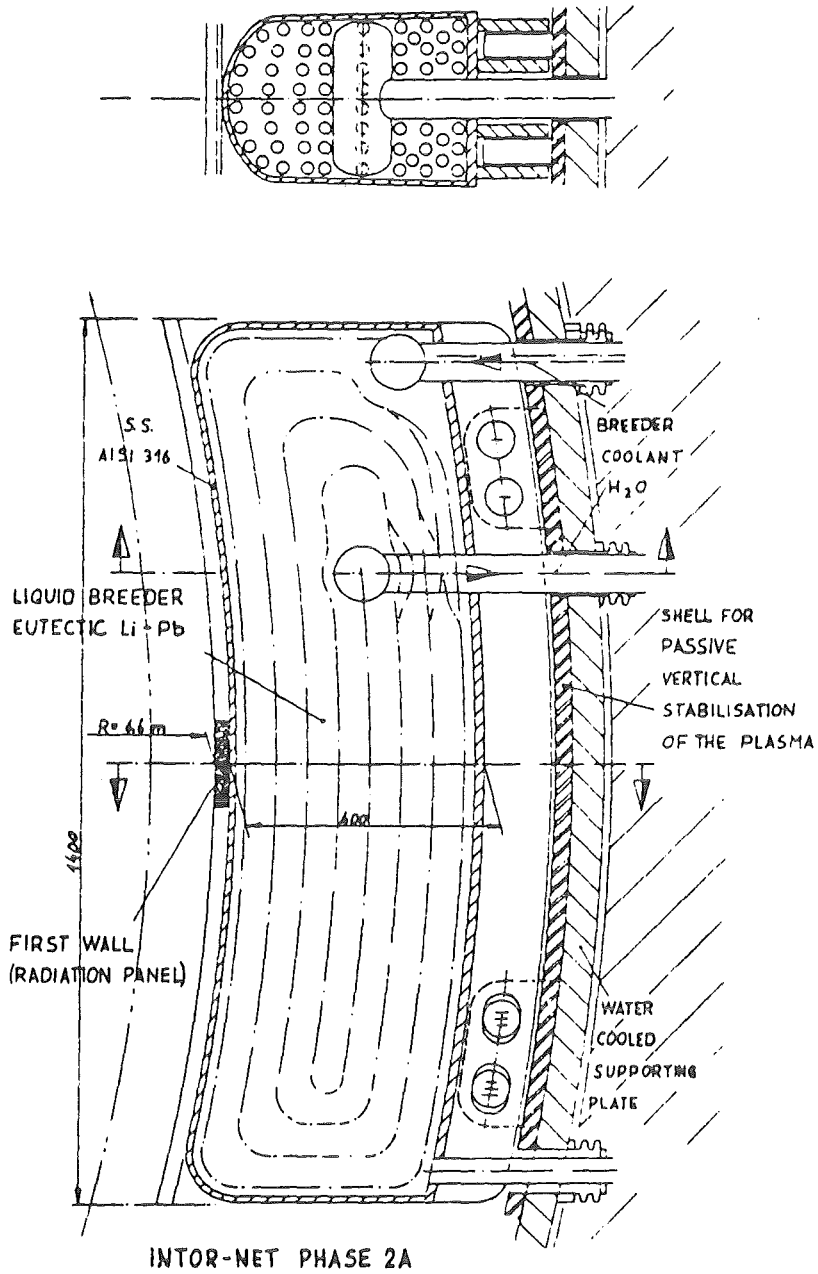


Fig. 13: Blanket cutaway according to ORNL design 1980.



INTOR-NET PHASE 2A
LIQUID BREEDING BLANKET UNIT

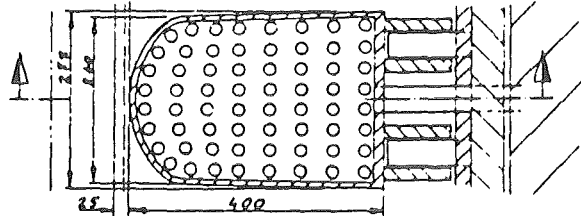
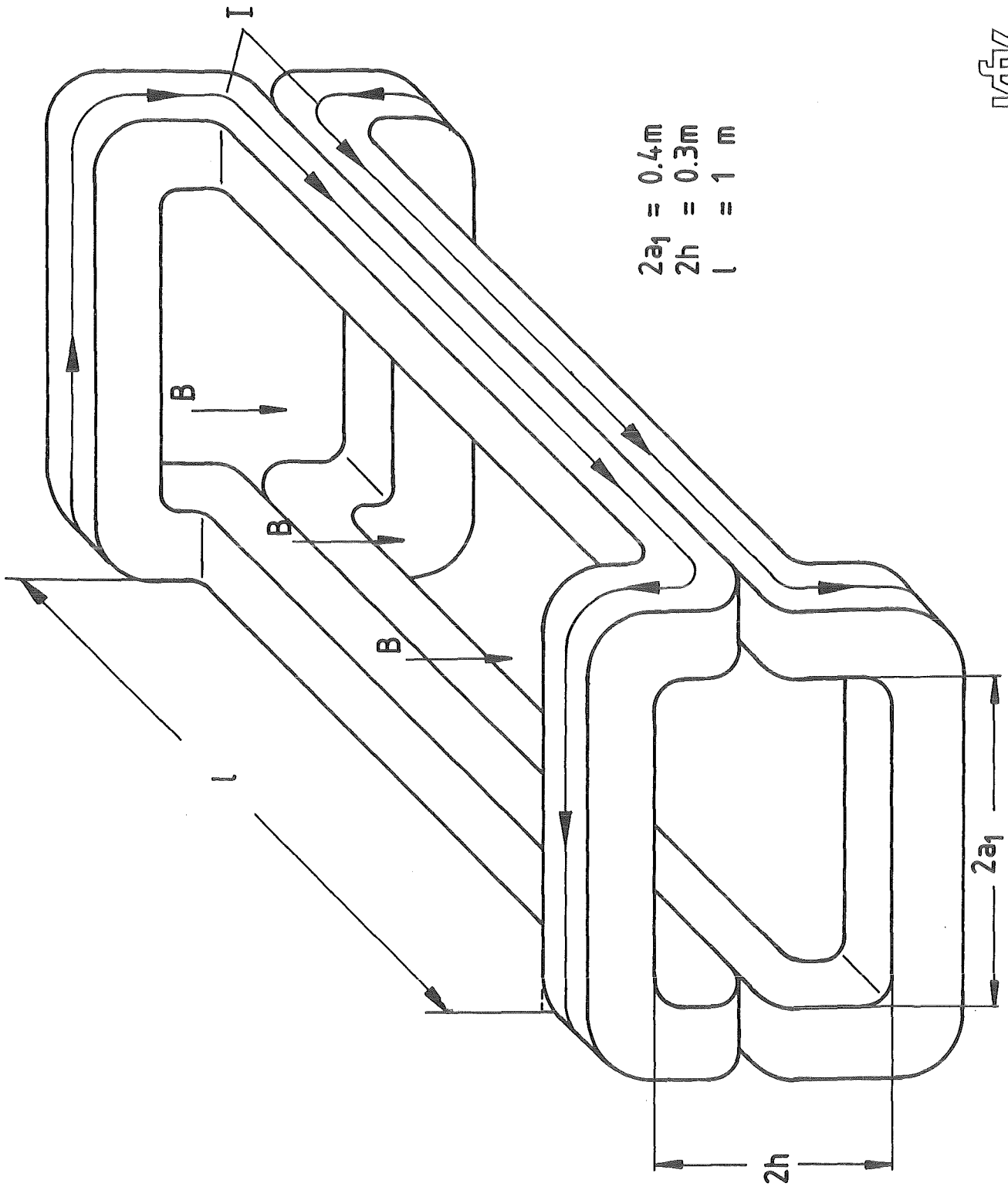


Fig. 14: INTOR IIa blanket



KfK

Fig. 15: Schematic representation of a dipole magnet.

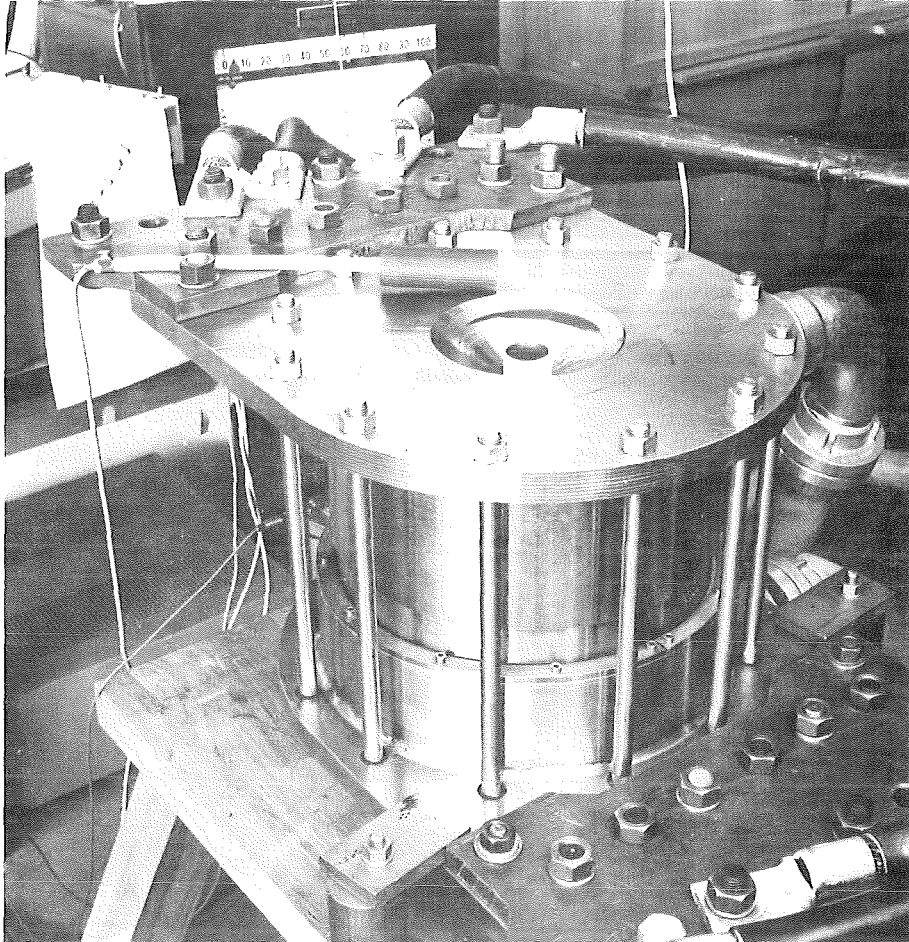


Fig. 16: 6.5 tesla magnet.